Paix *et al. Microbiome* (2025) 13:157
https://doi.org/10.1186/s40168-025-02146-2

Microbiome

RESEARCH

Open Access

Adaptive strategies of Caribbean sponge holobionts beyond the mesophotic zone

Benoît Paix[1,2*], Alexane Thivet[2], Celso Domingos[3], Özlem Erol[4], Niels van der Windt[2,5], Young H. Choi[4] and Nicole J. de Voogd[2,4*]

Abstract

Background Marine sponges and their microbiomes function together as holobionts, playing essential roles in ecosystem dynamics and exhibiting remarkable adaptability across depth gradients. This study utilized a multi-omics approach, integrating microbiome and metabolome analyses, to investigate adaptive strategies in sponge holobionts inhabiting the mesophotic (80–125 m), upper-rariphotic (125–200 m), and lower-rariphotic (200–305 m) zones of Curaçao. We hypothesized that depth-related environmental factors drive distinct adaptive strategies, similar to patterns observed in fish and coral assemblages.

Results Results revealed major differences in holometabolomes and microbial communities between Demospongiae and Hexactinellida sponges, reflecting class-specific adaptive strategies. Notably, phospholipid homeoviscous adaptation to temperature and pressure might emerge as a key mechanism in phosphorus metabolism. Adaptations in nitrogen metabolism were linked to diverse ammonia oxidizing archaea (AOA) symbionts, and dissolved organic matter cycling. Hexactinellid microbiomes exhibited intra-specific heterogeneity; however, species-specific associations with AOA symbionts such as *Cenarchaeum*and *Nitrosopumilus* were observed. Additionally, the lower-rariphotic hexactinellid holometabolomes highlighted the significance of the nested ecosystem concept through the identification of secondary metabolites produced by their associated fauna (aphrocallistins by zoanthids and xanthurenic acid by shrimp).

Conclusions This study highlights the ecological significance of sponge holobionts in mesophotic and rariphotic ecosystems, revealing diverse adaptations to unique physicochemical conditions and biotic interactions.

Keywords Multi-omics, Sponges, Microbiome, Metabolome, Depth, Rariphotic, Mesophotic, Demosponges, Hexactinellids, Adaptive strategies

*Correspondence:
Benoît Paix
benoit.paix@gmail.com
Nicole J. de Voogd
n.j.de.voogd@biology.leidenuniv.nl
[1] UMR CARRTEL, INRAE-Université Savoie Mont-Blanc, Thonon-Les-Bains, France
[2] Naturalis Biodiversity Center, Leiden, The Netherlands
[3] CIIMAR-Interdisciplinary Centre of Marine and Environmental Research, University of Porto, Avenida General Norton de Matos, S/N, Matosinhos 4450-208, Portugal
[4] Institute of Biology (IBL), Leiden University, PO Box 9505, Leiden 2333 BE, The Netherlands
[5] Institute of Environmental Sciences (CML), Leiden University, Leiden, The Netherlands

Background

Marine sponges (Phylum Porifera) are recognized as vital ecosystem engineers in benthic environments, providing essential ecological functions that support diverse marine life. Their highly efficient filter-feeding activity significantly contributes to the cycling of dissolved organic matter (DOM) and nutrient transfer within marine ecosystems [1, 2]. Sponges host a rich diversity of macrobenthic fauna [3–5] and complex microbial communities [6, 7]. Their associations with symbiotic microbes form a tightly integrated unit known as the holobiont [8–10]. Microbial symbionts play a crucial role by producing essential compounds such as vitamins [11, 12] and diverse secondary metabolites that function as chemical defenses against predators, competitors, and biofouling organisms [13, 14]. This functional diversity enables sponges to adapt to challenging environments, particularly under rising ocean temperatures [15] and ocean acidification [16, 17]. Moreover, sponge microbiomes facilitate the assimilation of specialized organic compounds, enabling survival in nutrient-poor environments [18, 19].

While these adaptations are relatively well-studied in shallow-water ecosystems, research on sponge microbiomes in mesophotic and deep-sea environments remains limited [20–22]. Expanding this knowledge is crucial to fully understand sponge adaptation and resilience in response to changing ocean conditions. In the mesophotic zone (30–150 m below sea surface), reduced light levels lead to shifts in sponge composition compared to shallow water sponges. While Demospongiae remain dominant in mesophotic sponge communities, their association with photosynthetic microbes declines. Instead, they rely more on heterotrophic and chemosynthetic symbionts, such as Chloroflexi and Acidobacteria, for nutrient acquisition and organic matter cycling [23, 24]. Beyond 200 m, glass sponges (class Hexactinellida) become more prevalent. Adapted to cold, high-pressure, and nutrient-limited conditions of deep-sea environments, these sponges form symbioses with specialized microbial taxa, such as ammonia-oxidizing archaea (AOA) and ammonia-oxidizing bacteria (AOB), which initiate nitrification by converting ammonium (NH_4^+) into nitrite (NO_2^-) [20, 21, 25]. Despite their ecological significance, the microbiomes of Hexactinellida remain poorly understood and exhibit a more heterogeneous microbial distribution than other Low Microbial Abundance (LMA) sponges [20, 25–27].

The rariphotic zone (150–300 m), first described in the Caribbean Sea by Baldwin et al. [28], serves as a transitional layer of reef-fish communities between the mesopelagic zone (twilight zone) and the bathypelagic zone (midnight zone). This zone refers to a specific depth range characterized by low irradiance levels, where light penetration becomes insufficient to support photosynthesis [28]. Recent observations also suggest a broadening of this delineation to other benthic communities on a wider scale in the Caribbean [29, 30]. However, it remains unclear how the rariphotic zone can influence other benthic communities beyond reef fishes. Historically, Caribbean sponge diversity has been primarily documented in shallow coral reef ecosystems [31], leaving the deep Caribbean reef slopes relatively unexplored. However, recent advancements in deep-sea exploration have led to the discovery of new species, including glass sponges emerging first in the rariphotic zone [32–34]. In particular, the community structure and functions of sponge microbiomes are poorly understood in rariphotic depths. Investigating these relationships could reveal novel insights into adaptive strategies, symbiotic interactions, and the production of bioactive compounds, especially under the unique environmental pressures of this transitional depth zone [13, 20].

To explore adaptive strategies, this study employed a multi-omics approach integrating microbiome and metabolome analyses to investigate sponge holobionts in mesophotic and rariphotic depths (Fig. S1). The reefs of Curaçao (Fig. S2) were selected as an ideal study site due to (i) the mesophotic-rariphotic delineation previously described in this area [28], and (ii) the coexistence of diverse Demospongiae and Hexactinellida communities, providing a unique opportunity to compare phylum-specific adaptive strategies [32]. This study aims to assess whether the mesophotic-rariphotic boundary, previously linked to low connectivity in fish and coral reef communities [28–30], also applies to sponges. We hypothesize that sponge classes exhibit distinct adaptive strategies below the mesophotic zone. These strategies could be driven by key metabolic pathways shaped by microbiome interactions in response to environmental gradients such as temperature, pressure, nutrient availability, oxygen concentration, and light limitation. Specifically, we expect that microbiome and metabolome profiles could co-vary with similar patterns observed along the photic zones. For instance, we hypothesize that variations in organic matter availability across photic zones could drive co-occurring shifts in the concentration of chemical markers and the abundance of microbial taxa involved in their uptake.

Sponge samples were collected from three defined photic zones: (i) mesophotic zone (80–125 m), (ii) upper-rariphotic zone (125–200 m), and (iii) lower-rariphotic zone (200-–305 m) [28]. Sponge samples were analyzed using a multi-omics workflow that combined 16S rRNA gene metabarcoding and UHPLC-HRMS metabolomics (Fig. S1), enabling a comprehensive assessment

of microbial and chemical diversity to uncover sponge adaptive mechanisms across depth gradients.

Methods

Sample collection and processing

A total of 60 sponge specimens were collected across four dives (Table S1): the first in October 2018 ($n = 2$), two in April 2022 ($n = 10$ and 34), and the final dive in March 2023 ($n = 14$). Sampling covered an area of approximately 0.5 km^2 off the Curaçao substation (12.083197 N, 68.899058 W, Fig. S2). Collections were conducted with the Curasub, a submersible equipped with two robotic arms for collecting sponge specimens, along with a compartmentalized basket and storage container for safe transport during dives (http://www.substation-curacao.com/). Sponges were collected from depths of 89 to 305 m, the latter being the maximum depth accessible by the Curasub. Specimens were initially identified by phylum during collection, resulting in 24 Demospongiae and 36 Hexactinellida samples. Specifically, 12, 5, and 7 demosponge specimens were collected from the mesophotic, upper- and lower-rariphotic zones, respectively. For Hexactinellida, 11 and 25 specimens were collected from the upper- and lower-rariphotic, respectively. Due to the logistical challenges of this sampling type and the patchy distribution, not all species could be collected in triplicate [35] (Table S1). Sponges were photographed both during collection and after retrieval to the surface (Fig. S3). Tissues were subsampled for morphological, molecular, and metabolomics analyses using sterilized tweezers and scalpel blades. Samples were immediately preserved in 5 ml tubes containing 96% ethanol and stored at − 20 °C until further processing. Extraction blanks for molecular and metabolomics analyses were prepared without sponge tissues. Additional samples of sponge-associated fauna (shrimps and zoanthids) were also photographed and preserved using the same protocol as the sponge specimens (Fig. S4).

DNA extractions

Sponge tissues were sectioned into pieces of approximately 3× 2× 1 mm, using sterilized tweezers and scalpel blades, yielding an average wet weight of 0.14 g (SD ± 0.02). Microbial and sponge DNA were extracted using the DNA™ SPIN Kit for Soil (MP Biomedicals, Inc.) following the manufacturer's instructions. The same protocol was applied to two DNA extraction blanks to monitor contamination. Additionally, DNA from Hexactinellida specimens was specifically extracted for barcoding identification using the DNeasy (Qiagen) Blood and Tissue Kit. All DNA extracts were stored at − 20 °C until further processing.

Sponge barcoding and morphological identification

Sponges were identified based on external morphology, spicules, and skeleton preparation following standard procedures and for Hexactinellida outlined by Reiswig & Stone [36], following identification keys from *Systema Porifera* [37] and checking all species with the World Porifera database [38].

For the barcoding of demosponges and sponge-associated fauna, the 28S rRNA gene was amplified using the primers 28S-C2-fwd and 28S-D2-rev [39], following the protocol described by Maslin, Paix et al. [40] (initial denaturation: 98 ℃ for 30 s, 30 cycles of denaturation at 98 ℃ for 10 s, 51 ℃ for 10 s, 72 ℃ for 15 s, and final extension of 72 ℃ for 5 min). PCR1 products were checked using E-Gel™ (agarose gels at 2%), and the absence of amplicons was validated for the negative controls and two extraction blanks. PCR1 products were cleaned using magnetic beads on the C.WASH plate washer (CYTENA, GmbH). PCR2 were performed with an initial denaturation step of 3 min at 95 °C followed by 15 cycles of 15 s at 95 °C, 15 s at 62 °C and 50 s at 65 °C, and a final extension step of 3 min at 65 °C. Samples from each plate were pooled by collecting 1 µl per sample using the OT-2 Liquid Handler (Opentrons Labworks, Inc.) and cleaned using NucleoMag NGSBeads. End-repair and dA-tailing were performed on the pools using the NEBNext Ultra II End Prep Kit, followed by another clean-up. The DNA concentration of the pooled samples was quantified using a TapeStation 4150 (Kit HSD 5000, Agilent Technologies, Santa Clara, CA, USA) in combination with the Qubit dsDNA BR assay kit (Thermo Fisher Scientific, USA) to take forward an equimolar mass to the native barcode ligation step, performed using the NEB Blunt/TA Ligase Master Mix. Pools were then combined, followed by an AMPure XP bead clean-up (0.4 ×ratio). Lastly, native adaptors for sequencing were ligated using the NEBNext Quick ligation kit, and a final quantification of the library was performed on the Qubit Flex. The final library size was set up to 12 µl at 10–20 fmol for sequencing on a Nanopore R10.4.1 flow cell. Consensus sequences were generated by assembling raw reads using NGSpeciesID 0.3.0 and medaka 1.8.0.

For hexactinellids, PCR amplifications were conducted following the protocol of Dohrmann et al. [41], using the primers 16S1fw and 16SH_mod for the amplification of the 16S rRNA gene [42, 43]. The resulting PCR products were sequenced via Sanger sequencing by STABVIDA using the BigDye Terminator v 3.1 kit on an ABI 3730XL DNA analyser (Applied BiosystemsTM, Foster City, CA, USA).

The sequences generated were analyzed using the Basic Local Alignment Search Tool (BLAST) (https://www.ncbi.nlm.nih.gov/genbank/) to assess similarity

with existing sequences in public databases and confirm the taxonomic placement of the species.

Library preparation and high throughput sequencing for 16S rRNA gene metabarcoding

The library preparation for metabarcoding analyses was conducted through a two-step PCR protocol for all samples, two extraction blanks, and a negative control. For PCR1, the V4-V5 regions of the bacterial and archaeal 16S rRNA gene were targeted with the 515 F-Y/926R primers [44]. These primers were chosen according to a preliminary validation step resulting in a highly similar archaeal community composition compared to the archaeal-specific Uni519 F/1000R [45, 46], previously used for other Hexactinellida samples [20] (details provided in Supplementary information). PCR1 reactions were performed with the KAPA HiFi HotStart Ready Mix PCR Kit (Roche Molecular Systems, Inc.) in a T100 Thermal Cycler (Bio-Rad, Hercules, CA, USA). The following thermal cycling scheme was set up: initial denaturation at 95 °C for 3 min, 30 cycles of denaturation at 98 °C for 20 s, annealing at 50 °C for 30 s, followed by extension at 72 °C for 30 s. The final extension was carried out at 72 °C for 5 min. PCR1 products were checked using E-Gel™ (agarose gels at 2%), and the absence of amplification was validated for the negative controls and two extraction blanks. PCR1 products were then cleaned using NucleoMag NGS-Beads (bead volume at 0.9 times the total volume of the sample, Macherey Nagel, Düren, Germany) and the VP 407 AM-N 96 Pin Magnetic Bead Extractor stamp (V&P Scientific, San Diego, CA, USA). PCR2 were performed using IDT xGen™ NGS Adapters & Indexing Primers kit (Integrated DNA Technologies, Inc.) with an initial denaturation step of 3 min at 95 °C followed by 8 cycles of 20 s at 98 °C, 30 s at 55 °C and 30 s at 72 °C, and a final extension step of 5 min at 72 °C. Successful labeling of PCR2 products was then checked with the Fragment Analyzer Agilent 5300 using the DNF-910–33 dsDNA Reagent Kit (35–1500 bp) protocol (Agilent Technologies, Santa Clara, CA, USA) and concentration was determined with PROSize 3.0 software. Using the QIAgility (Qiagen, Hilden, Germany), samples were pooled together at equimolar concentration. The pool was then cleaned using NucleoMag NGSBeads and the DNA concentration was quantified using Tapestation 4150 (Kit HSD 5000, Agilent Technologies, Santa Clara, CA, USA). The amplicon pool was sent to BaseClear (BaseClear B.V., Leiden, The Netherlands) for MiSeq Illumina sequencing (V3 2*300 PE platform).

16S rRNA gene metabarcoding data processing and analyses

The raw reads were initially processed by BaseClear B.V. for demultiplexing (using bcl2fastq version 2.20, Illumina), and filtering based on two quality controls (using Illumina Chastity filtering, and a PhiX control signal filtering). The resulting reads were then analyzed using the DADA2 workflow for the inference of Amplicon Sequence Variant (ASV) [47, 48], using the "dada2" R package following the workflow described in Callahan et al. [49] and guidelines described in the online tutorial (https://benjjneb.github.io/dada2/tutorial.html). Filtering and trimming parameters were set as follows: truncation length of 270 bp and 240 bp for forward and reverse reads, respectively, maxN =0, maxEE =2, and truncQ =2. After constructing the ASV table, chimeric sequences were filtered and removed and the taxonomic assignment was performed using the Silva v138 reference database [50]. In alignment with the SILVA v138 taxonomy, the phylum Crenarchaeota was used instead of Thaumarchaeota which was reassigned at the class level as Nitrososphaeria [51]. The ASV and taxonomy tables produced by the pipeline were then combined into a phyloseq object, together with the sample metadata table, using the "phyloseq" R package [52]. The dataset was subsequently filtered by removing all sequences from Eukaryota, chloroplast, and mitochondria (representing 0.2%, 0.1% and 0.9% of all reads, respectively). Data was then decontaminated with the negative controls and extraction blanks used as control samples, through the "decontam" R package with the "prevalence" method [53]. 16 contaminant ASVs (out of 14,922 ASVs in total) were detected and removed from the dataset. Rarefaction curves are plotted through the "vegan" R package [54]. The α-diversity metrics were estimated using Chao1 (estimated richness), Pielou (evenness), and Shannon (both richness and evenness) indices on the rarefied dataset (rarefaction to the minimum library size, i.e., 10,926 reads), using the "phyloseq" and "vegan" R packages [52, 54]. According to the Shapiro tests, the diversity metrics significantly differed from the normal distribution. Consequently, the significance of the diversity metrics across the different groups of samples was investigated through non-parametric tests (Kruskal–Wallis followed by pairwise Wilcoxon tests) using the "agricolae" R package [55]. Following recommendations for compositional approaches [56, 57], all other analyses were conducted without rarefaction, using the "phyloseq" R package, and the datasets normalized to the total number of sequences per sample (named "compositional dataset"). The β-diversity was analyzed with non-metric multidimensional scaling (NMDS) using Bray–Curtis dissimilarity. Differences in β-diversity between groups

were statistically checked with one-way permutational multivariate analysis of variance (PERMANOVA) tests followed by pairwise Adonis tests, using the "vegan" R package. Differential analyses were performed using the "metacoder" R package [58], to identify the significant taxa differentially abundant according to the comparisons (i) between the two sponge classes, and (ii) among the photic zones for both classes separately. The differential analyses were performed with a subset of the compositional dataset excluding rare ASV (relative abundance < 0.04%).

Extraction, sample preparation, and data acquisition for UHPLC-ESI-HRMS metabolomics

Samples of sponge tissues filled with 96% EtOH, were sonicated for 30 min. The extract was then concentrated with the CentriVap Benchtop Vacuum Concentrators (Labconco™, Kansas City, MO, USA). Fresh 96% EtOH was added to the sponge tissues, and the sonication-evaporation procedure was repeated twice. Extracts were transferred to 1.5 ml glass vials and stored at − 20 °C until the sample preparation for metabolomics.

UHPLC-MS samples were prepared by solubilizing 2 mg of dried sample in 0.5 ml of methanol (HPLC grade, Sigma-Aldrich, St. Louis, MO, USA). Ten quality control (QC) samples were prepared by mixing all the samples at equimolar concentrations, in addition to ten extraction blanks, and two analytical blanks. Samples and blanks were injected in a random order, with a QC for every five injections. The samples were analyzed using a UHPLC-DAD-HRMS, UltiMate 3000 system (Thermo Scientific, Waltham, MA, USA) coupled to a QTOF-II mass spectrometer equipped with an electrospray ionization (ESI) source (Bruker, Bremen, Germany). The separation was performed using a 2.1 mm × 150 mm, 2.6 µm Kinetex C18 column (Phenomenex, Torrance, CA, USA) at 40 °C and a 0.3-ml/min flow rate. For samples, QC and MeOH, 1 µL was injected and eluted with a gradient of 0.1% formic acid in water (A) and 0.1% formic acid in acetonitrile (B) starting at 5% B (0–30 min), 98% B (30–35 min) and equilibrated at 5% B for 5 min. The capillary voltage was set at 4000 V, the drying temperature at 350 °C (0.3 ml/min); the nebulizer gas pressure at 2.0 bar, and the gas drying at 8.0 ml/min. The samples were analyzed in positive mode using a scan range of 100–1600 *m/z*.

Metabolomics data processing, statistical analysis, and annotation

The UHPLC-MS/MS raw data files obtained were first converted into mzML files using the open-source msConvert tool from ProteoWizard library (http://proteowizard.sourceforge.net). The mass detection, chromatogram alignment, and ion deconvolution were performed using Metaboscape (Bruker Daltonics GmbH, Bremen, Germany, version 4.0) following the T-ReX 3D processing workflow (Version 1.9, detailed settings provided in Supplementary information). Briefly, the software performed automated mass calibration and deisotoping, followed by alignment of the resulting feature retention times using a LOESS-based alignment algorithm. The resulting feature table was filtered through an in-house R script [59], to remove successively experimental and analytical bias according to signal/noise ratio (using blanks), coefficient of variation (using QCs), and coefficient of correlation (using samples). The α-chemodiversity was analyzed through the data matrix normalized to the sum of the chromatographic peak areas, using the Shannon index and the vegan R package. Differences in α-chemodiversity within groups were tested through an ANOVA test, using the vegan R package. Multivariate analyses were analyzed using MetaboAnalyst 6.0 online web tool [60], through normalization to the sum of the chromatographic peak areas, a log10-transformation, and a Pareto scaling. Through a first Principal Component Analysis (PCA), QC samples were confirmed to be grouped, and blanks were identified as outliers. A second PCA was then conducted with the sponge samples only, to determine the overall clustering patterns of the holometabolome chemodiversity. Statistical differences in metabolome profiles between the sample groups were assessed with a PERMANOVA test and the Euclidean distance with the vegan R package. Following PCA, partial least square discriminant analyses (PLS-DA) were conducted to reveal the most discriminant features involved in the differences between (i) the sponge class and (ii) the photic zones. Using retention time and MS/MS spectra, the annotation efforts were dedicated to these features with a VIP score > 2 for the class differences, and VIP score > 3 for the zone differences for both classes. These thresholds were defined to select only significant features, according to ANOVA and *t*-tests. The annotation of this discriminant feature list was facilitated by the Feature-Based Molecular Network (FBMN) to identify clusters of compounds sharing similar MS/MS spectra and fragmentation patterns. The mass spectrometry data were first processed with Metaboscape and the results were exported to Global Natural Products Social Molecular Networking (GNPS; [61]) for FBMN analysis. The data was filtered by removing all MS/MS fragment ions within ± 17 Da of the precursor *m/z* MS/MS spectra were window filtered by choosing only the top 6 fragment ions in the ± 50 Da window throughout the spectrum. Parameters used for building the FBMN within GNPS are detailed in the Supplementary information (SI). The FBMN was

finally analyzed using the Cytoscape software (version 3.10.2). The level of confidence in the annotation of the *m/z* features was determined according to Schymanski et al. [62].

Multi-omics integration of metabarcoding and metabolomics datasets

Shannon measures from both metabarcoding and metabolomics datasets were compared and their correlation was tested using the Spearman rank correlation using the "ggpubr" R package [63]. A Procrustes analysis was performed using the metabolomics and metabarcoding dissimilarity matrices through the "vegan" R package. For the metabolomics, the dissimilarity matrix was calculated with the Euclidean distance and corresponded to the target matrix (X matrix). For the metabarcoding, the Bray–Curtis index was used to calculate the matrix to be rotated (Y matrix). Following the Procrustes analysis, a Mantel test was performed to confirm the significance of the correlation between the two dissimilarity matrices. Both datasets were also analyzed together into a supervised multi-omics analysis to assess the co-occurrences of the most discriminant ASVs and metabolites according to the discriminations between the depth zones and sponge classes. To conduct this approach, the DIABLO analysis was performed with the "mixOmics" R package through the *block.splsda*() function [64, 65]. The supervision factor gathered the samples according to their respective depth zone and sponge class (resulting in 5 groups: mesophotic demosponges, upper-rariphotic demosponges, lower-rariphotic demosponges, upper-rariphotic hexactinellid, and lower-rariphotic hexactinellid). An optimal number of six components was obtained based on the performance plot calculated for validation of the DIABLO model. The tuning step of the DIABLO pipeline resulted in optimal numbers of 25, 5, 5, 5, 5 ASVs and 6, 20, 30, 5, 30, 5 metabolites to retain for the first six components. Using this final DIABLO model, the resulting heatmap was obtained and plotted using the *cimDIABLO*() function, to visualize distinct clusters of samples gathered according to the co-occurrence of discriminant variables.

Results

Morphological and molecular identification of sponges and associated fauna specimens

The analysis of the demosponge samples identified 13 distinct species across 11 genera, eight families, and five orders (Table S1, Fig. S3). The most diverse group was the order Tetractinellida with a total of nine species belonging to four families: *Aciculites higginsii* Schmidt, 1879 (family Scleritodermidae), *Gastrophanella implexa* Schmidt, 1879 (family Siphonidiidae), *Geodia* cf. *megastrella* Carter, 1876, *Geodia* aff. *curacaoensis* van Soest, Meesters, Becking, 2014, two unidentified *Geodia* sp., *Calthropella (Pachataxa) lithistina* [66], *Penares mastoideus* [66] (family Geodiidae), *Cinachyrella kuekenthali* [67] (family Tetillidae); followed by the order Haplosclerida; *Neopetrosia eurystomata* van Soest, Meesters, Becking, 2014; *Petrosia* aff. *weinbergi* and two unidentified *Petrosia* sp. (family Petrosiidae); order Biemnidae, *Biemna microacanthosigma* Mothes, Hajdu, Lerner and van Soest, 2004 (family Biemnidae); Order Scopalinida *Svenzea zeai* [68] (family Scopalinidae) and the order Suberitida: *Topsentia ophiraphidites* [69] (family Halichondriidae).

The analysis of hexactinellid samples revealed 7 distinct species across 7 genera, distributed among 5 families (Table S1, Fig. S3). The most diverse family was Sceptrulophora *incertae sedis*, which included three species: *Lefroyella* sp., *Conorete pourtalesi* Reiswig & Dohrmann, 2014, and *Verrucocoeloidea liberatorii* Reiswig and Dohrmann, 2014. Additionally, each of the following families was represented by one species: *Heterotella* sp. nov (family Euplectellidae), *Myliusia* sp. (order Hexasterophora *incertae sedis)*, *Dactylocalyx pumiceus* Stutchbury, 1841 (family Dactylocalycidae), and *Hexactinella* sp (family Tretodictyidae).

The analysis of sponge-associated fauna revealed the presence of zoanthids colonizing three glass sponges: *C. pourtalesi*, *V. liberatorii,* and to a lesser extent *Hexactinella* sp. (Fig. S4). For the three sponges, these zoanthids specimens corresponded to *Vitrumanthus schrieri* Montenegro and Reimer, 2022 based on their 28S rRNA gene sequences. Shrimp pairs were found inhabiting internal cavities of *C. pourtalesi* specimens, and were identified as *Eiconaxius caribbaeus* [70] based on morphological analyses (pers. comm. Charles Fransen).

Diversity and composition of prokaryotic communities

Rarefaction curves reached a plateau for all samples (Fig. S5 A), indicating a good coverage of the richness through the number of reads obtained for the whole study. Among the α-diversity metrics of the sponge-associated prokaryotic communities, the Pielou (evenness) and Shannon (richness and evenness) indices were significantly higher for Demospongiae compared to Hexactinellida samples (Kruskal–Wallis followed by post-hoc Wilcoxon tests: $p < 0.001$ for both indices, Fig. S5B). For Chao1, no significant differences were observed when comparing the two sponge classes (post-hoc Wilcoxon test: $p > 0.05$, Fig. S5B). For the three indices, no significant differences were observed between photic zones, either within Demospongiae or Hexactinellida (post-hoc Wilcoxon test: $p > 0.05$, Fig. S5B).

The β-diversity, investigated through the Bray–Curtis dissimilarity index using an NMDS analysis, revealed two distinct class-specific clusters separated along the first axis with Demospongiae samples on the left side, and Hexactinellida samples on the right side (Fig. 1A, B). Differences between the two classes were confirmed to be significant through the two-way PERMANOVA tests followed by pairwise comparison tests ($p < 0.01$, Tables S2 and S3). For the Demospongiae, the NMDS and PERMANOVA analyses also revealed distinct clusters between the three photic zones (Fig. 1A, Table S3), while no differences were observed within the Hexactinellida samples. When depth is fitted as a continuous factor within the NMDS analysis, increasing gradients (from 100 to 300 m) can be distinguished (Fig. 1) but towards opposite directions along the NMDS1 axis for each class (i.e., right side for Hexactinellida and left side for Demospongiae). Significant differences were observed when comparing the β-diversity among sponge genera (Tables S4 and S5). Clusters being specific to the sponge species can be observed on the NMDS plot (Fig. 1B), for example with *D. pumiceus* and *V. liberatorii* for the hexactinellids, as confirmed by the multivariate pairwise comparison test (Table S5).

The NMDS plot displaying ASV scores (Fig. 1C), revealed the presence of dominant archaeal ASVs

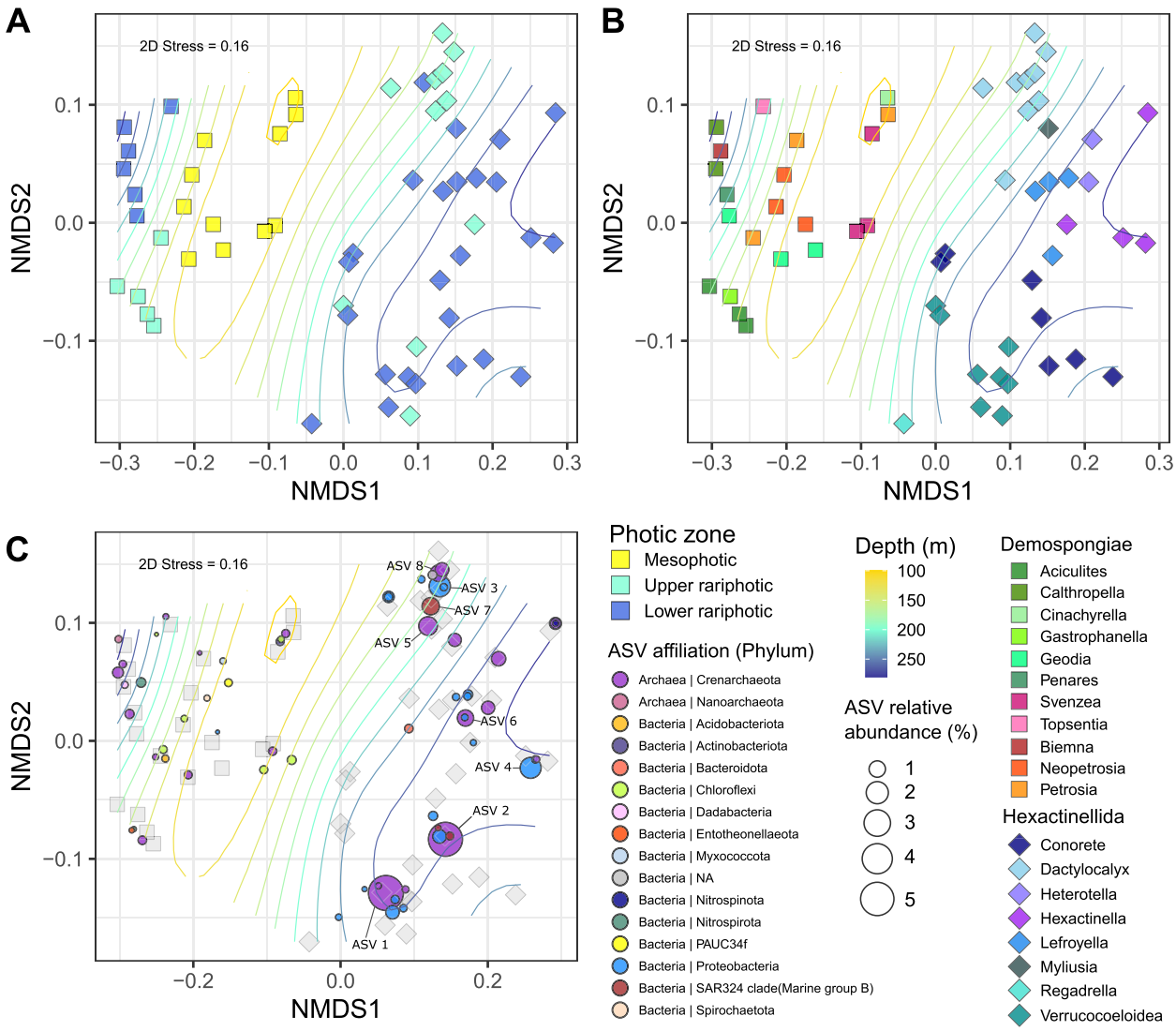

Fig. 1 NMDS plots (built with the Bray–Curtis dissimilarity index) representing the β-diversity of the prokaryotic communities associated with the Demospongiae and Hexactinellida samples. **A** and **B** Plots of the sample scores. **A** Color codes were represented according to the photic zones. **B** Color codes were represented according to the sponge genus. **C** Plot of the ASVs scores. Color codes were represented according to the prokaryotic phyla. **A**, **B**, and **C** Curved lines represent the fitting of the depth gradient using the *ordisurf* function

(Crenarchaeota with relative abundances > 1% in the overall dataset) associated with the Hexactinellida cluster. More precisely, the two most abundant ASVs; ASV1 and ASV2 (both with relative abundance > 5%) were found to be specifically associated with the deepest rariphotic samples collected (~ 250–300 m), within the *V. liberatorii* and the *C. pourtalesi* cluster, respectively (Fig. 1B, C). Within the other Hexactinellida samples (*Mylusia*, *Dactylocalyx*, *Hexactinella*, *Lefroyella*), distinct ASVs from Crenarchaeota were found (e.g. ASV5, ASV6, ASV8), in addition to Proteobacteria (ASV3 and ASV4) and SAR324 (ASV7). These ASVs were found in lower abundance than ASV1 and ASV2 (ranging from 1% to 1.8%). ASVs found specifically associated with Demospongiae were observed in lower abundance (< 1%), and mostly affiliated (i) to the PAUC34f, and Chloroflexi for the mesophotic and upper-rariphotic ones, and (ii) to Crenarchaeota for the lower-rariphotic ones.

The prokaryotic community composition plotted at the family level confirmed the major differences observed between Demospongiae and Hexactinellida samples (Fig. S6). Within the Demospongiae, Chloroflexi and Crenarchaeota were the two dominant phyla, represented by an unaffiliated family from the SAR202, and the Nitrosopumilaceae, respectively. To a lesser extent, other families were also dominant, such as Nitrospinaceae (Nitrospinota phylum), Nitropiraceae (Nitrospirota phylum), Nitrosococcaceae (Proteobacteria phylum), two unaffiliated families from the Acidobacteriota phylum, and an unaffiliated family from the PAUC34f phylum. For hexactinellids, higher intra- and inter-specific variation can be observed compared to demosponges (Fig. S6). Among this heterogeneous composition within Hexactinellida species, Crenarchaeota and Proteobacteria were confirmed as dominant phyla. The Nitrosopumilaceae was the dominant archaeal family with a wide range of relative abundance varying from 1.24 to 83.75%, without clear host species or depth zone-specificity. Species-specific proteobacterial families can be distinguished, for example with an unaffiliated family of the UBA10353 group for *Hexactinella* sp., and the PS1 clade from the Parvibaculales for *V. liberatorii*. For archaea, host species-specificity could be discerned when analyzing their specific composition at the genus level (Fig. S7). More precisely, *Cenarchaeum* was the dominant genus of *C. pourtalesi* and *V. liberatorii*, while *D. pumiceus* and *Leyfroyella* sp. were found to harbor unaffiliated members of the Nitrosopumilaceae family. These latter were also dominant within the upper-rariphotic Demospongiae, while the mesophotic sponges (except *C. kuekenthali* and one *N. eurystomata*) were dominated by Candidatus *Nitrosopumilus.*

The heat tree performed with all samples highlighted a large diversity of taxa differentially abundant between the two sponge classes across all taxonomic levels (Fig. S8, Table S6). The analysis confirmed our previous observations for the most abundant bacterial taxa found in significantly higher abundance within Demospongiae (Fig. S6), with (i) Chloroflexi (Dehalococcoidia and Caldilineaceae), (ii) Nitrospirota (*Nitrospira* genus), (iii) Acidobacteriota (Vicinamibacterales), and (iv) Entotheonellaeota (Entotheonellaceae). Within the Hexactinellida the bacterial taxa found significantly and differentially more abundant for this class were (i) the Planctomycetota (Phycisphaeraceae and Pirellulaceae), (ii) the Enterobacterales (*Vibrio* genus), (iii) the cyanobacterial genus Prochlorococcus MIT931, and (iv) the Bacteroidia (more specifically the *Fulvitalea* genus). Within the Crenarchaeotal family Nitrosopumilaceae, the Candidatus *Nitrosopumilus* genus was found to be significantly and differentially more abundant in Demospongiae, while *Cenarchaeum* was found specifically more abundant in Hexactinellida (Fig. S8).

The differential pairwise analyses conducted with the Demospongiae samples revealed a large diversity of taxa being specific to each photic zone (Fig. 2, Table S6). Demospongiae sponges from the mesophotic zone were enriched with SAR202 and Caldilineaceae (both from the Chloroflexi phylum), Spirochaetota, and more specifically its genus *Spirochaeta*, Vicinamibacterales, and Candidatus *Nitrosopumilus.* Below the mesophotic, the families Microtrichaceae, Entotheonellaceae, Nitrosococcaceae, and Woeseiaceae were found to be more abundant within the upper-rariphotic zone. In addition, the lower-rariphotic demosponges were specifically enriched in Dadabacteriales, Thermoanaerobaculaceae, the TK10 cluster from the Chloroflexi phylum, and the *Cenarchaeum* from the Nitrosopumilaceae (Fig. 2). For the Hexactinellida samples (Fig. S9, Table S6), a large diversity of taxa was also found differentially abundant for the upper and lower-rariphotic zones respectively. More precisely, the upper-rariphotic Hexactinellida sponges were enriched in Leptospiraceae, *Prochlorococcus*, Rhodobacteraceae, SAR11 Clade Ia, *Coxiella*, while lower-rariphotic ones were enriched with *Vibrio*, *Fluvitalea*, Phycisphaeraceae, and *Cenarchaeum* (Fig. S9).

Chemical diversity and annotation of sponge-holobiont metabolomes

Demosponge holometabolomes were characterized by a significantly higher α-chemodiversity (Shannon index) compared to their hexactinellid counterparts (ANOVA test: $p < 0.05$). However, no significant differences were observed among the photic zones (ANOVA test: $p > 0.05$, Fig. S5C). PERMANOVA and

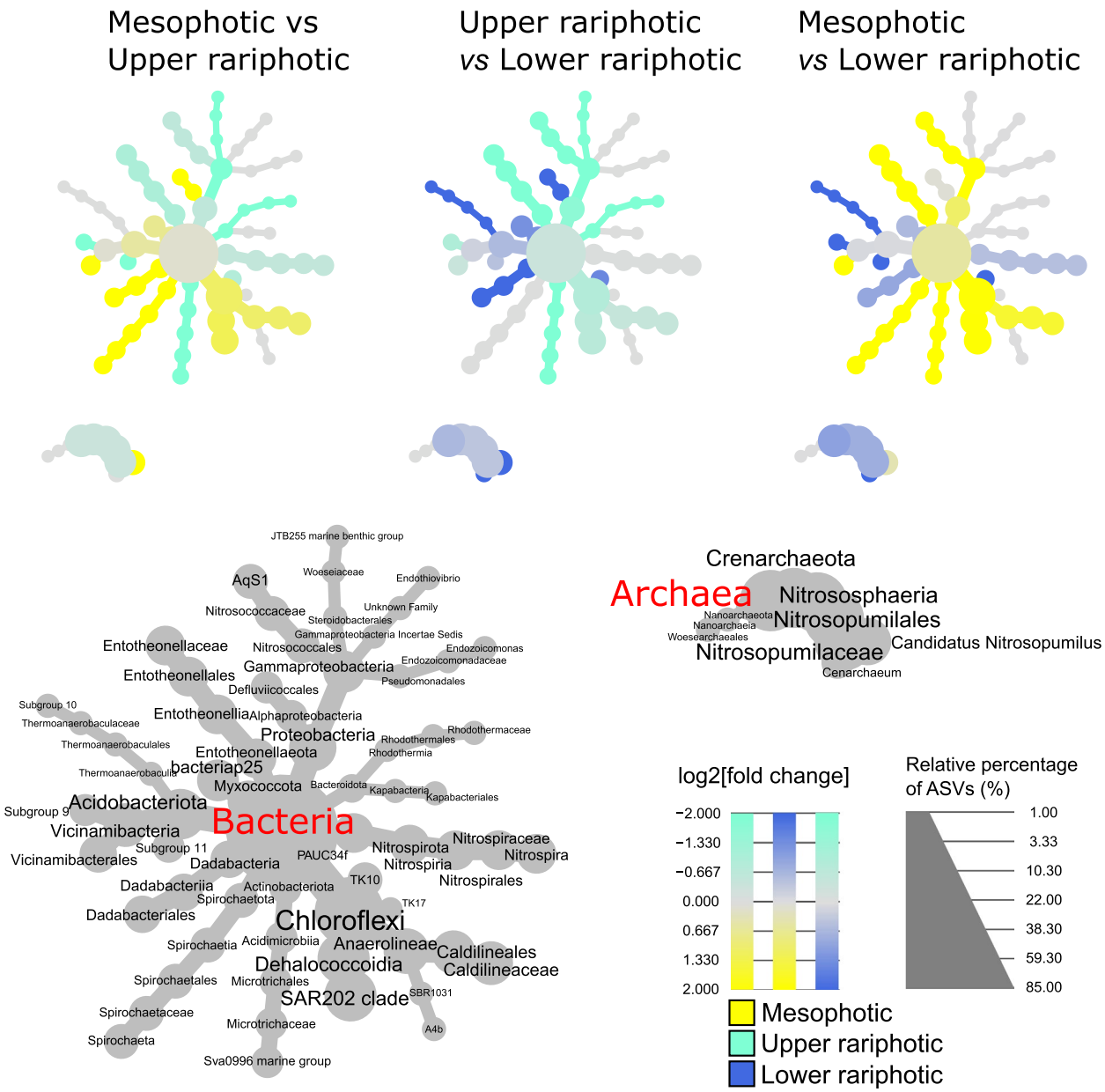

Fig. 2 Phylogenetical heat trees performed with Demospongiae samples, and representing taxa significantly and differentially abundant between mesophotic, upper-rariphotic, and lower-rariphotic samples. For each taxon, **i** the colors of their associated nodes correspond to the log2 fold change between the ratio of the mean relative abundance within samples of each zone, **ii** and the size of their nodes corresponds to their relative abundance

pairwise comparison tests revealed significant differences between the metabolome profiles of the two sponge classes, as confirmed by the PCA plot (Fig. 3A, Tables S2 and S3). For Demosponges, mesophotic and lower-rariphotic samples appeared clustered separately on the PCA plot. Significant differences were confirmed among the photic zones for this class, through the two-way PERMANOVA test followed by a pairwise comparison test (Tables S2 and S3). For hexactinellids, no clear differences among the photic zones or depth gradient can be observed, according to the PCA plots and tests (Fig. 3A, Table S2). Within demosponges, the PCA plot did not reveal clear genus-specific clusters of holobiont metabolome profiles (Fig. 3B). However, differences between species can be observed for hexactinellid samples, as also suggested by the

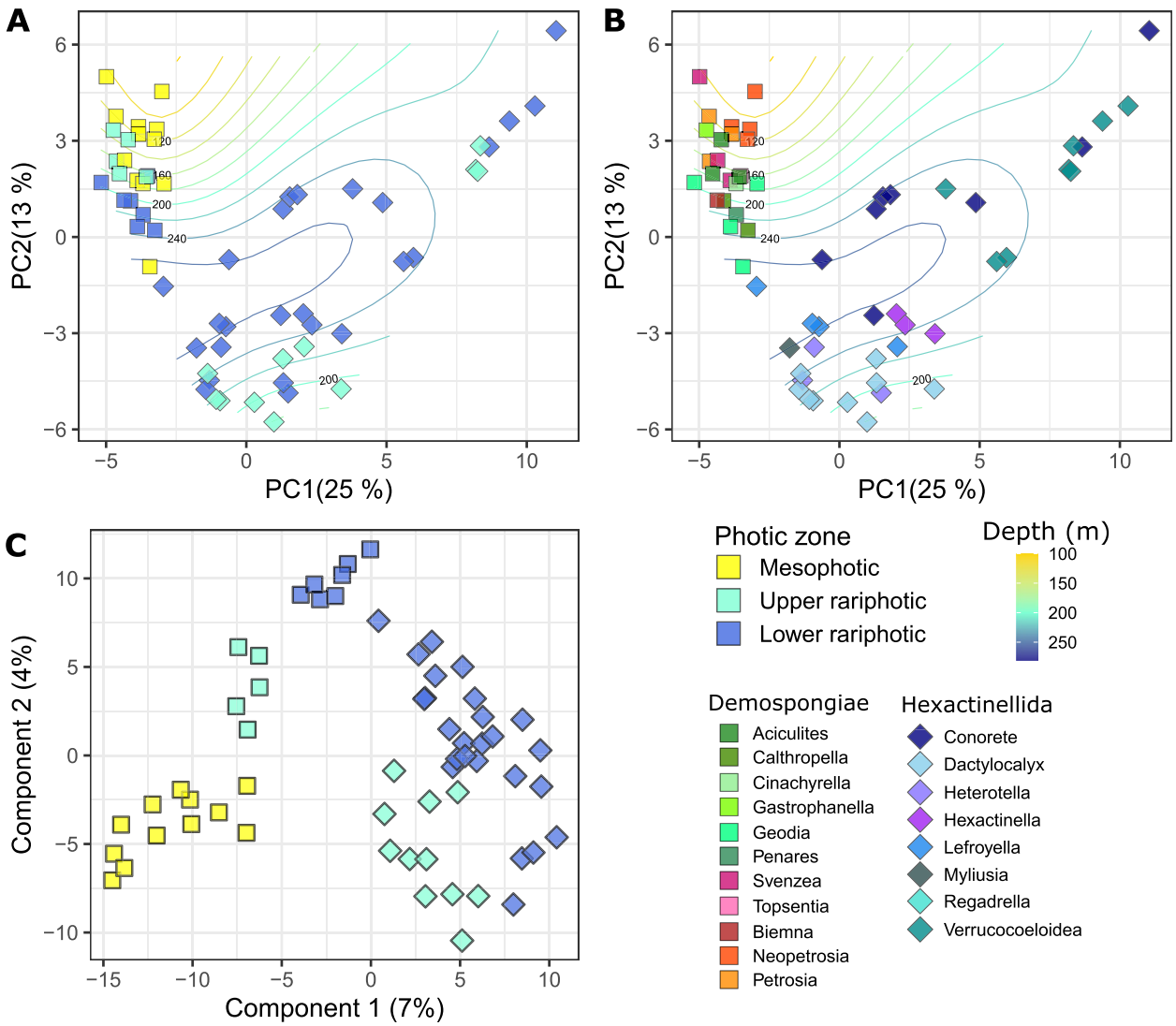

Fig. 3 Plots of multivariate analyses of the metabolome associated with the Demospongiae and Hexactinellida holobionts. **A** and **B** PCA plot of the metabolomes. Curved lines represent the fitting of the depth gradient using the *ordisurf* function. **A** Color codes are defined according to the photic zones. **B** Color codes are represented according to the sponge genus. **C** PLS-DA plot conducted with the photic zone as a supervised factor

PERMANOVA and pairwise comparison tests (Fig. 3B, Tables S4 and S5).

PLS-DA were conducted to confirm the presence of metabolites significantly involved in the discrimination between the sponge class or photic zone, and target the annotation strategy specifically towards these compounds. In addition to the major differences between the sponge classes, discriminations within the photic zones were also observed with a continuous shift from the mesophotic to the lower-rariphotic zones (Fig. 3C). PLS-DA performed with Demospongiae and Hexactinellida samples separately and with the photic zone as a supervision factor, also revealed discrimination between photic zones (Fig. S10).

These PLS-DA allowed to establish a list of the most discriminant features (VIPs) between (i) Demospongiae and Hexactinellida (Table S7, VIP scores > 2), (ii) photic zones for the Demospongiae samples (Table S8, VIP scores > 3), and (iii) photic zones for the Hexactinellida samples (Table S9, VIP scores > 3). Annotation efforts were focused on these compounds, and facilitated through a first identification step of the main chemical families, using the molecular networking approach. The FBMN allowed the gathering of the MS/MS fragmented

ions within distinct clusters associated with specific chemical families (Fig, S11). The annotation was first focused on clusters gathering VIPs (Figs. S12 and S13). Cluster A represented the main cluster of the overall FBMN, gathering a total of 12 phosphatidylcholines (PC), together with 12 *lyso*-PCs corresponding to a specific sub-cluster (Fig. S12). PC and *lyso*-PCs were annotated based on the characteristic fragment ion of phosphocholine at *m/z* 184.07 $[C_5H_{15}NO_4P]^+$ [71]. Fragment ions associated with the carbon chains allowed the identification of their acyl chain length and unsaturation number, for both PCs and *lyso*-PCs (Fig. S12). Cluster G gathered compounds characterized by typical 1:2:1 isotopic pattern indicating the presence of two bromine atoms (Fig. S13). The isotopic cluster at *m/z* 539.0407 and 541.0402 (corresponding to $[M+H]^+$ and $[M+H+2]^+$, respectively) matched with the chemical formula $C_{20}H_{24}Br_2N_6O_2$. The MS/MS fragmentation patterns confirmed the identification of aphrocallistin, a dibrominated alkaloid previously isolated and characterized by Wright et al. [72] from the glass sponge *Aphrocallistes beatrix* (Fig. S14, Table S7). Other compounds from cluster G were linked to aphrocallistin with a very similar MS/MS fragmentation pattern (Fig. S13). These compounds corresponded to aphrocallistin derivatives, such as *m/z* 569.0453 corresponding to the chemical formula $C_{21}H_{26}Br_2N_6O_3$ (Fig. S12). Cluster D was also found to share a similar mass spectrum to the dibrominated compounds of cluster G, especially with the identification of an aphrocallistin fragment ion, and a brominated purinone (*m/z* 286.0286, chemical formula: $C_9H_{12}BrN_5O$). Cluster I gathered peaks with MS/MS spectra sharing a neutral loss of *m/z* 141.02 (Fig. S12). This fragmentation pattern is characteristic of the phosphatidylethanolamines (PEs), with the loss of the phosphoethanolamine moiety [71, 73]. A total of 2 PEs and 7 *lyso*-PEs were identified from this cluster. Finally, cluster O was characterized by features putatively annotated as amino acid derivatives (Fig. S11, Tables S8 and S9).

Among the 28 first VIPs (VIP score >2) discriminating demosponge from hexactinellid holometabolomes, 12 were putatively annotated as phospholipids, including 9 *lyso*-PCs (Table S7). Among them, *lyso*-PC(C17:0), *lyso*-PC(O-C17:0), *lyso*-PC(C17:1), and *lyso*-PC(O-C18:0) were found to have higher abundance within the Demospongiae samples (T-test: $p < 0.001$ for all, Fig. 4A, Table S7). Conversely, *lyso*-PC(C20:4), *lyso*-PC(C18:0), *lyso*-PC(C20:5), *lyso*-PC(C19:0), and *lyso*-PC(C20:1) were found to discriminate the two classes with higher abundance within Hexactinellida (*t*-test: $p < 0.001$ for all, Fig. 4A, Table S7).

Additionally, the other phospholipids putatively identified as *lyso*-PI(C19:0) and *lyso*-PI(C18:0) were found as discriminant compounds with higher abundance in Demospongiae, while higher abundance within Hexactinellida was observed for *lyso*-PE(C20:4) (Fig. 4A, Table S7). Aphrocallistin and one of its derivatives (VIP n°25 corresponding to $C_{21}H_{26}Br_2N_6O_3$) were both characterized by a discriminant higher abundance in Hexactinellida sponges compared to Demospongiae (Fig. 4A). These compounds also revealed distinct normalized concentrations within the different Hexactinellida genera, with higher concentrations observed within *V. liberatorii*, *C. pourtalesi*, and *Hexactinella* sp. (Fig. S15). A compound identified as xanthurenic acid (Fig. S16), was also discriminant between the two classes with significantly higher concentrations for Hexactinellida samples (Fig. 4A), and more specifically within *C. pourtalesi* (Fig. S15). Discriminant differences within photic zones for Demospongiae samples were observed for *lyso*-PC(O-C18:0), PC(O-C18:0/O-1:0), Gln-Lys, and Gln-Pro with higher abundance within the lower-rariphotic zone compared to the mesophotic one (Fig. 4B, Table S8). Conversely, rhodosamine and salsolinol were found to be discriminant with relative concentration decreasing with the depth. Within Hexactinellida, the 17 first VIPs involved in the discrimination between the upper and lower-rariphotic zones (VIP scores >2), were essentially identified as phospholipids and dipeptides (Table S9). VIPs annotated as *lyso*-PS(C15:1), *lyso*-PC(C22:5), *lyso*-PE(C22:2), *lyso*-PE(C22:4), *lyso*-PE(C20:4), Leu-Leu, and Leu-Val were discriminant with significantly higher abundance in the upper-rariphotic zone (Fig. 4C, Table S9). Conversely, a higher abundance of xanthurenic acid was observed in the lower-rariphotic zone, as *C. pourtalesi* were only found in this specific zone (Fig. 4C, Table S9).

Multi-omics analyses of metabarcoding and metabolomics datasets

A weak but significant linear correlation was observed between the Shannon measures of both datasets (Pearson correlation: $r = 0.34$, $p = 0.011$). This correlation was mainly driven by the differences between the two sponge classes (Fig. 5A). Similarly, a significant correlation was also confirmed between the distance matrices of both datasets (Mantel tests $r = 0.22$, $p = 0.002$), being also driven by sponge class differences (Fig. 5A, B). Additionally, *V. liberatorii* and *C. pourtalesi* samples appeared to be clustered together, and separately from the rest of the other hexactinellids samples (Fig. 5C). The heatmap built through a multi-omics supervised analysis (DIABLO), revealed a total of 135 co-occurring discriminant features (44 metabolites and 91 ASVs) involved in the differences between the samples grouped in their respective class and photic zones. The hierarchical clustering confirmed the major differences between the two classes, but also

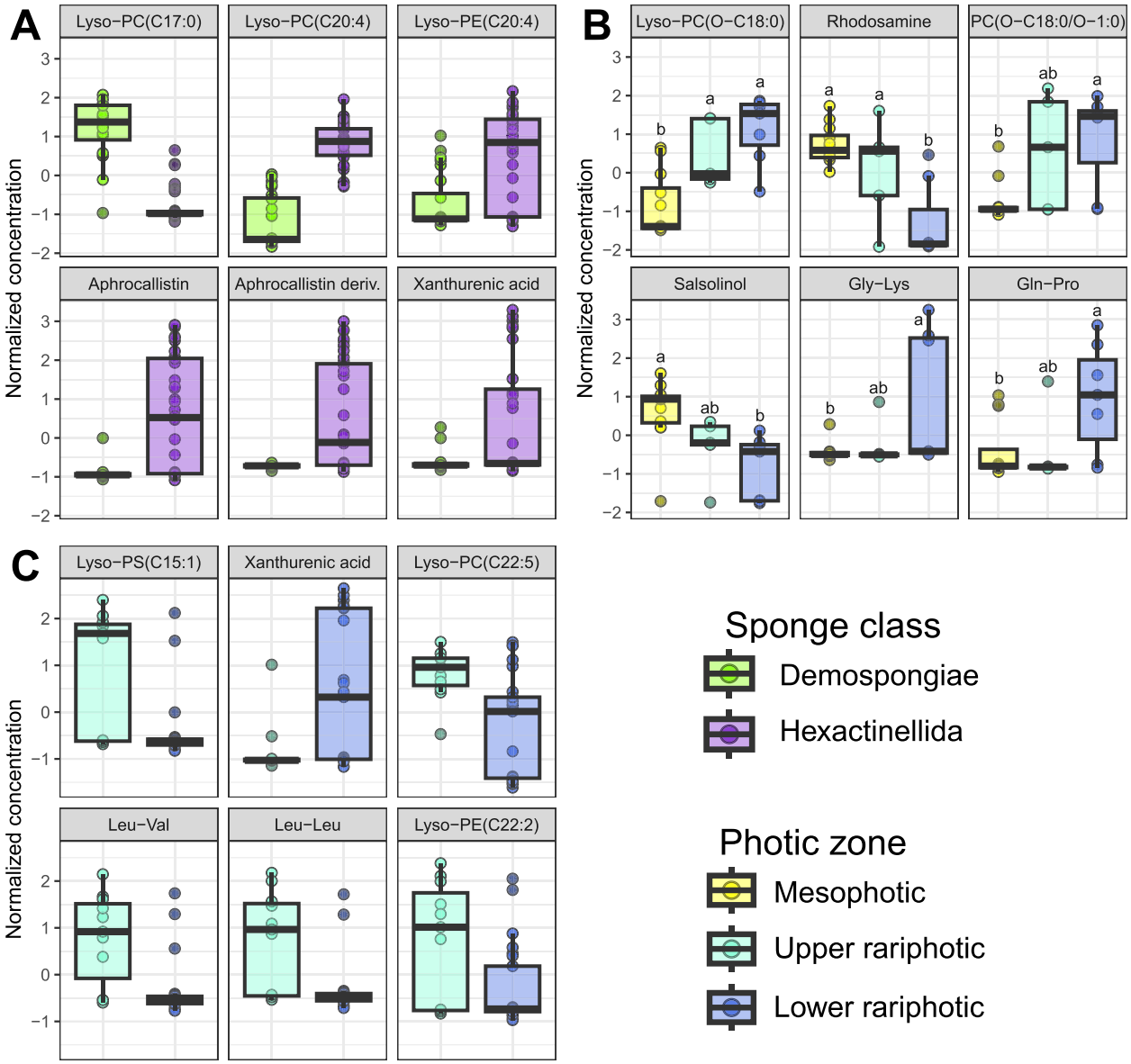

Fig. 4 Normalized concentrations of discriminant metabolites putatively annotated with a confidence level ≥ 2. **A** Discriminant metabolites (VIPs scores > 2, $p < 0.0001$) according to the sponge classes. **B** Discriminant metabolites (VIPs scores > 3, $p < 0.05$) according to the photic zones for Demospongiae samples. Lowercase indices correspond to Tukey's HSD pairwise comparison test. **C** Discriminant metabolites (VIPs scores > 3, $p < 0.05$) according to the photic zones for Hexactinellida samples. Results from the ANOVA and *t*-tests are presented in Tables S7, S8, and S9

the differentiation between the photic zones. Chloroflexi and Actinobacteriota ASVs were clustered together with ether-linked *lyso*-PCs and derivatives of amino acids and amino sugars (e.g., dipeptides and rhodosamine), with higher abundance in the demosponges holobionts. A second cluster sharing ASVs and metabolites being differentially more abundant in the *C. pourtalesi* samples revealed *Cenarchaeum* and SAR324 Marine group B ASVs, together with primary lipids and the xanthurenic acid. Finally, hexactinellids were characterized by a higher abundance of several long-chain *lyso*-PCs [e.g., *lyso*-PC(C20:4) and *lyso*-PC(C20:5)], and aphrocallistins as previously observed in the VIP analyses.

Discussion

Major differences in host-microbiome adaptive strategies are observed between the sponge classes

Whether analyzed independently or through a multi-omics analysis, the overall holometabolome profiles and prokaryotic community structure revealed major

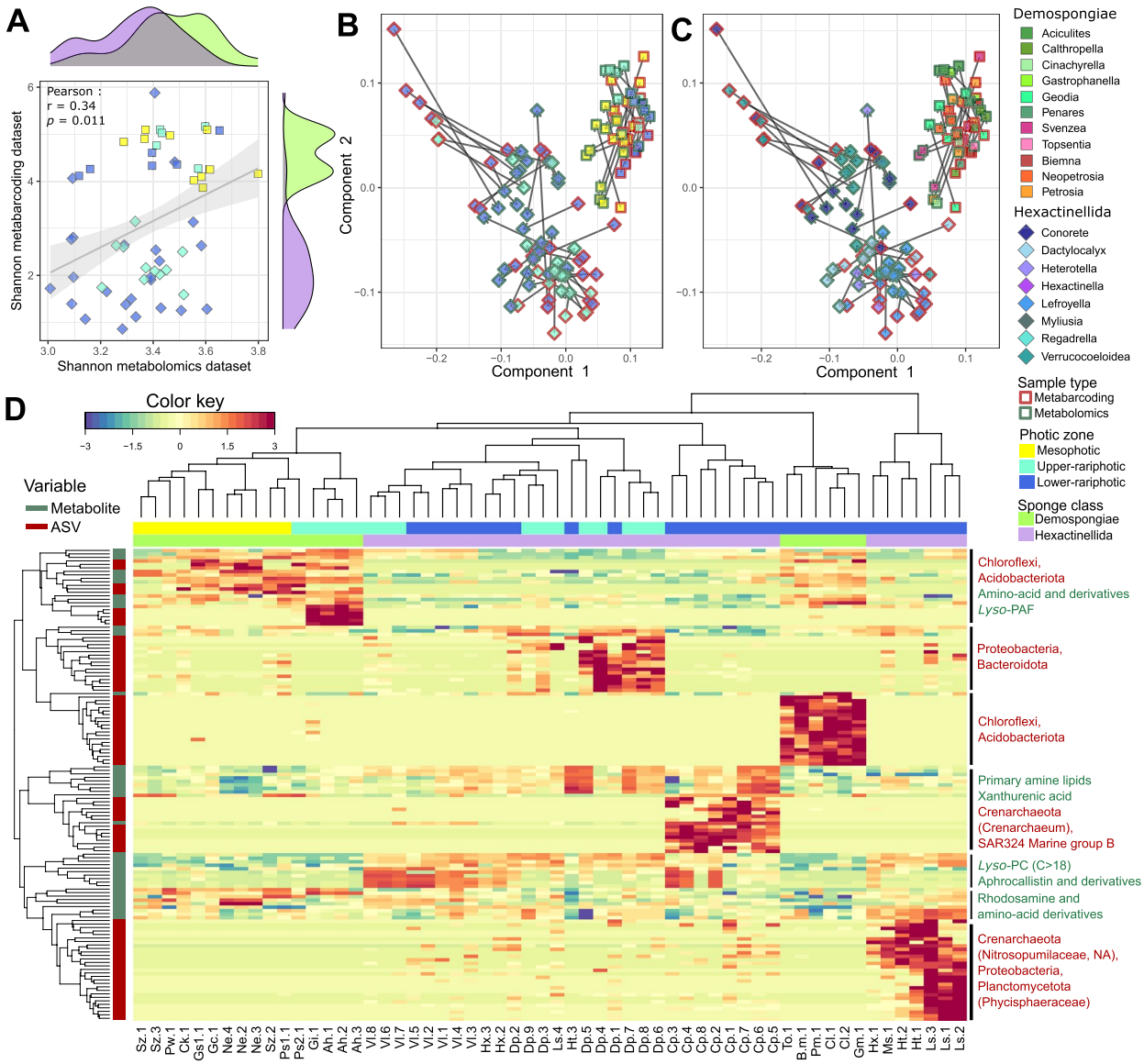

Fig. 5 Multi-omics analysis of the sponge holobionts integrating metabarcoding and metabolomics datasets. **A** Comparison of Shannon indices obtained through the metabarcoding and metabolomics dataset. **B** Plot of the Procrustes analysis performed with both datasets, displaying the color codes for the photic zones. **C** Plot of the Procrustes analysis performed with both datasets, displaying the color codes for sponge genera. **D** Heatmap of the supervised multi-omics analysis (DIABLO). Sample names and abbreviations are listed in Table S1

differences between sponge classes. Similar patterns have been observed in deep-sea sponge microbiomes in the South Pacific Ocean off the coast of New Zealand [20], and more broadly in the Atlantic Ocean [26]. In our study, all demosponge samples exhibited a high microbial abundance (HMA)-like community composition dominated by the phyla Chloroflexi, Acidobacteriota, and PAUC34f [23]. In contrast, hexactinellid samples displayed lower evenness and an LMA-like structure, primarily dominated by a few Gammaproteobacteria and Crenarchaeota ASVs. These class-specific differences in microbial composition and abundance, emphasize the need to consider distinct host-microbiome adaptive strategies in deeper marine environments. Notably, hexactinellids also exhibited lower chemical α-diversity (Shannon index), which might be explained by a lower microbial richness and consequently a lower diversity of microbial-derived metabolites.

The relationships between the datasets, based on α-diversity measures (Shannon index measures) and multivariate analyses (Mantel test, Procrustes, and DIABLO analyses) appeared primarily driven by class-level

differences, but limited within each class. This finding suggests limited functional redundancy between demosponge and hexactinellid microbiomes, but indicates partial redundancy within each class. Using a multi-omics approach that combined metabarcoding and metabolomics, similar patterns were observed at lower taxonomic levels in four Mediterranean sponge holobionts, where intraspecific correlations were weaker than interspecific ones [74]. Functional redundancy has also been proposed in metagenomics studies of HMA sponges from Caribbean coral reefs [75], and in metatranscriptomic analyses of deep-sea sponges [22]. In this latter study, functional redundancy was suggested to contribute to the holobiont stability, supporting adaptation to extreme environments. However, the functional redundancy concept in marine microbiomes is increasingly debated, as many microbial functions remain uncharacterized or underestimated [76]. Therefore, evaluating the correlation between overall taxonomical and functional diversity as done in our study, offers a crucial "annotation-free" approach to investigate functional redundancies beyond reliance on a limited set of known functions [76].

Due to the unbalanced nature of this study dataset, with no Hexactinellida occurring in the mesophotic zone and a limitation in the species specimens collected for lower-rariphotic demosponges (Table S1), the depth effect was not analyzed both classes together. Consequently, samples from both sponge classes were analyzed separately, with cautions taken when comparing strategies between species. Clear differences in the overall variance of microbiome β-diversity and holometabolome patterns were observed across depth zones for demosponges. In contrast, for hexactinellids, which are restricted to depths below the mesophotic zone (Fig. 6A), no distinct separation between the upper and lower-rariphotic zones was evident. However, supervised analyses revealed a wide diversity of discriminant metabolites and prokaryotic taxa specifically associated with these depth zones in both sponge classes. We propose that these microbial and chemical markers offer valuable insights into the adaptive strategies of sponge holobionts in response to depth-related environmental factors such as temperature, light, pressure, nutrients, oxygen, and biotic interactions (Fig. 6B–H). A critical aspect of this study focused on the MS/MS annotation of these discriminant metabolites, to uncover their potential biosynthetic origins and ecological roles using literature reviews and reference databases (e.g., Lotus, MarineLit). While untargeted metabolomics can provide valuable information to supplement phylogenetic studies of glass sponges [77], this research presents the first untargeted metabolomics dataset for hexactinellid samples investigated through annotation efforts.

Temperature, pressure, and phosphate availability shape distinct phospholipidome adaptations

Phospholipids (PLs) and *lyso*-PLs (LPLs) emerged as the most diverse group of compounds identified in the sponge holometabolome extracts, including various forms of PCs, *lyso*-PC, PE, *lyso*-PE, and *lyso*-PS. These phospholipid classes are widely reported as dominant membrane components in many sponges, though their relative abundance can vary greatly between species [74, 78]. Among these membrane lipids, PLs and LPLs are also essential roles in sponge adaptation to environmental changes [78]. Specifically, LPLs function as membranes-signaling metabolites, involved in various cell processes including growth, proliferation, survival, and apoptosis [79]. In sponges, LPLs may contribute to embryogenesis and morphogenesis [80, 81]. Among the annotated PLs and LPLs of our study, several were characterized as ether-linked *lyso*-PCs, PCs, and PEs, such as *lyso*-PC(O-C17:0), *lyso*-PC(O-C18:0) and PC(O-C18:1/O-C1:0). These lipids, previously identified in other marine sponges [80–82], are also named "platelet-activating factors" (PAFs). PAFs are known for their wide range of biological activities in marine invertebrates [83–85]. In shallow water sponges, PAF production has been linked to immune responses, functioning as immunolipids in the antibacterial defense mechanism of *Suberites domuncula* [85]. Additionally, PAFs may serve also as antifouling agents deterring settlement by ascidians, bryozoans, barnacles, algae, and mussels as observed in the Australian sponge *Crella incrustans* and the Mediterranean sponge *Oscarella tuberculate* [80, 86]. In this study, *lyso*-PC(O-C17:0) and *lyso*-PC(O-C18:0) were specifically associated with Demospongiae samples, and higher concentrations of *lyso*-PC(O-C18:0) and PC(O-18:1/O-1:0) detected in rariphotic sponges (Fig. 6B). While the ecological role of PAFs in the rariphotic sponges remains unclear, further research is necessary to explore their potential function as immunolipids, particularly in shaping host-specific and depth-specific microbial communities.

Interestingly, *lyso*-PCs identified as biomarkers for demosponges contained either one or no unsaturation and short acyl chains (below C17). In contrast, the other *lyso*-PCs identified as hexactinellid biomarkers exhibited a higher unsaturation degree (up to five double bonds) and longer acyl chains (from C18 to C20). We propose that the membranes of hexactinellid sponge species, or their associated bacteria, may be specifically adapted to the rariphotic zone, by producing long-chain polyunsaturated *lyso*-PCs. This adaptation likely mitigates the negative effects of lower temperatures and higher pressures on the membrane fluidity (Fig. 6C). This process, known as homeoviscous adaptation, has been widely observed across diverse deep-sea phyla, including Chordata,

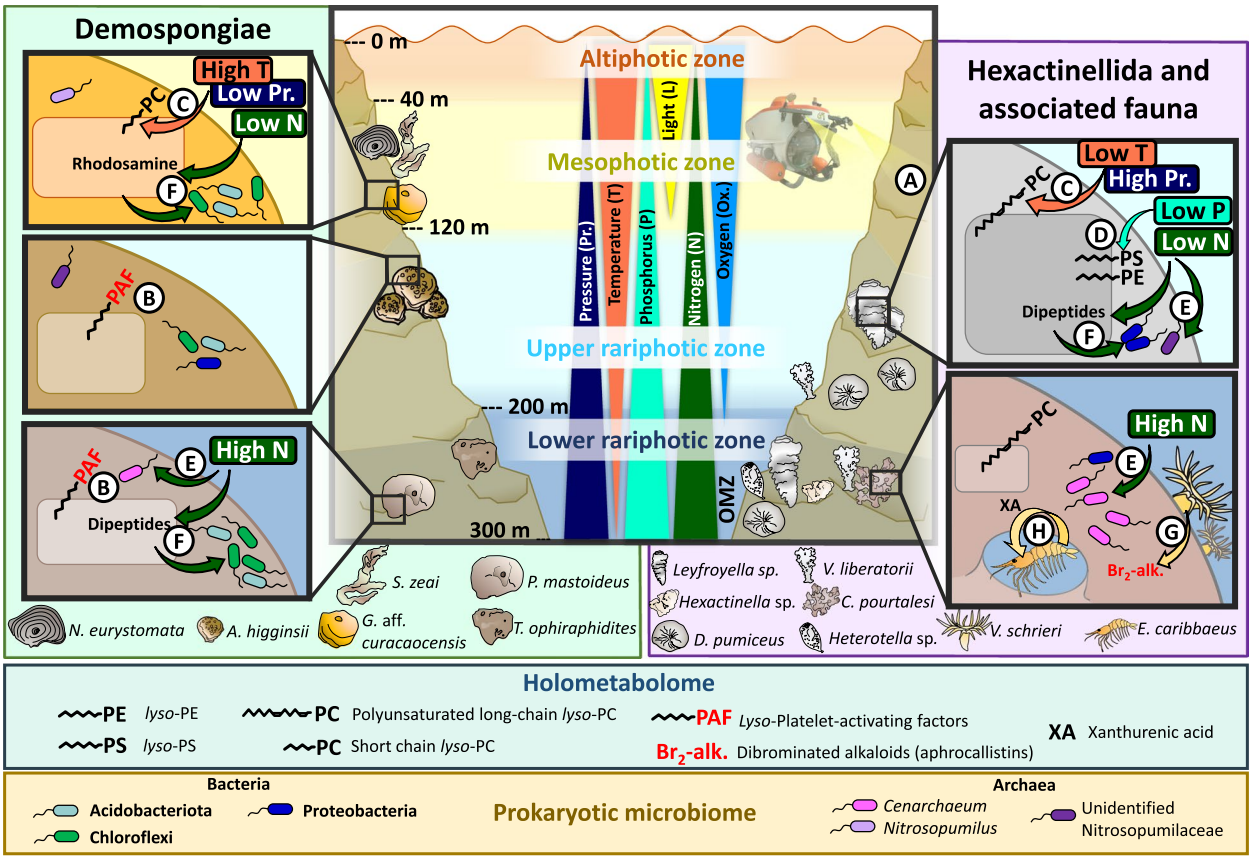

Fig. 6 Summary of the distinct adaptive strategies of sponge holobionts collected within the mesophotic and rariphotic zones. **A** No hexactinellids were occurring in the mesophotic zones, suggesting a preferential adaptation up to the lower-rariphotic zone. **B** *Lyso*-PAF are produced as immunolipids in the rariphotic demosponges. **C** Homeoviscous adaptation of the *lyso*-PCs: the chain might be longer under lower temperatures and higher pressure within hexactinellids, to increase the membrane fluidity. The opposite situation could be observed in most of the demosponges holophospholipidome rather adapted to shallower conditions. **D** The diversity of phospholipids synthesis pathways is suggested to increase as an adaptation to overcome the lower P-concentrations, leading to more diverse PLs classes. **E** Within hexactinellids, the AOA members of the Nitrosopumilaceae family appear host-specific at the sponge species level and could be vertically transmitted. AOA symbionts such as *Cenarchaeum* are expected to ensure ammonia detoxification through its oxidation, under the Oxygen Minimum Zone (OMZ). **F** Amino sugars (e.g., rhodosamine) and amino acid derivatives (e.g. dipeptides) might constitute a major source of DON for microbial members of the sponge holobionts, including the Chloroflexi. **G** The zoanthid *Vitrumanthus schrieri* produces dibrominated alkaloids from the aphrocallistin family acting as chemical defense for the sponge hosts *C. pourtalesi*, *V. liberatorii* and *Hexactinella* sp. **H** The shrimp *Eiconaxius caribbaeus* inhabiting cavities of the hexactinellid *C. pourtalesi* might produce xanthurenic acid as an endogenous molting inhibitor to keep their body size small enough, maintaining their adult life cycle within the sponge. Metabolites in red correspond to putative chemical defenses (*lyso*-PAF as immunolipids, and aphrocallistin as brominated alkaloids)

Arthropoda, Cnidaria, and Ctenophora [87–89], as well in the shallow water phototrophic sponge species *Phyllospongia foliascens* (as *Carteriospongia foliascens* in Bennett et al. [90]). Further studies through controlled conditions have to be considered for sponge holobionts to better decipher if these differences in phospholipid profiles are either linked to a direct environmental adaptation to the depth, or a distinct evolutionary history.

Nutrient concentrations, including phosphate, are known to increase with depth reaching a maximum between 500 and 1000 m. This pattern results from higher nutrient demand in the oligotrophic euphotic zone, and the downward transport of particulate organic matter into the deep ocean via the biological pump [91]. As a result, varying phosphorus availability may drive distinct phosphorus cycling strategies in sponge-holobionts leading to differences in phospholipid composition, a pattern already observed in planktonic communities [92]. In this study, hexactinellids in the upper-rariphotic zone exhibited a more diverse composition of phospholipid classes, with elevated concentrations of *lyso*-PE and *lyso*-PS in addition to the *lyso*-PC. This finding suggests that sponge-holobionts might diversify their phosphorus-uptake pathways

under conditions of low phosphorus availability by producing multiple PL classes (Fig. 6D).

Ammonia oxidation and DOM cycling as key pathways of the N-metabolism within mesophotic and rariphotic depths

The nitrogen metabolism homeostasis of sponge holobionts is regulated by diverse prokaryotic symbionts involved in key nitrogen cycling processes, including nitrogen fixation, nitrification, denitrification, and anaerobic ammonium oxidation processes [93]. Among these, ammonia oxidizing archaea (AOA) and nitrite oxidizing bacteria (NOB) are particularly well-adapted and dominant within cold-water and deep-sea sponge holobionts [20, 25, 94], playing crucial roles in the nitrification process [95]. However, there is no clear consensus regarding the species-specificity of these symbionts in deep-sea sponges. For instance, weak species-specificities were observed among samples from the South Pacific Ocean and Cantabrian Sea, suggesting a random acquisition of archaeal symbionts [20] and the prevalence of functional redundancy within the microbiome [22]. Conversely, Amplicon Sequence Variants (ASVs) from the AOA Nitrosopumilaceae family were identified as species-specific in deep-sea demosponges and hexactinellids from the Campos Basin, Southern Brazil) implying potential vertical transmission of these symbionts [21]. In shallow water sponges, vertical transmission has also been suggested. For example, nitrifying symbionts such as Candidatus *Nitrosokoinonia* and Candidatus *Nitrosymbion* have been identified in *Coscinoderma matthewsi* [95], and the AOA *Cenarchaeum symbiosum* has been found across various sponge species in the Western Pacific, Caribbean, and Mediterranean Sea [96–98]. Consistent with the findings of Steinert et al. [20], our study confirmed significant heterogeneity in the relative abundance of Crenarchaeota, within hexactinellid species. However, this observation is based on compositional data at the phylum and family levels, where relative abundances were analyzed with the bacterial community. When examining archaeal composition at the genus and ASVs level, species-specific patterns became evident. For example, *Cenarchaeum* was represented by two distinct ASVs, each predominantly associated with *C. pourtalesi* and *V. liberatorii*, respectively. Additionally, other ASVs from an unidentified Nitrosopumilaceae genus were specifically occurring within *D. pumiceus* and *Leyfroyella* sp. These findings suggest that the hexactinellid-AOA association is likely driven by a deterministic process, such as a vertical acquisition of a dominant host-specific nitrifying symbiont. However, once these symbionts are established their proliferation and relative abundance may be heavily influenced by external stochastic factors resulting in variability within the overall prokaryotic community. To confirm the early vertical acquisition hypothesis, and the metabolic role of AOA in rariphotic sponges, further analyses need to be considered for example through complementary omics, microscopy approaches, and the use of seawater controls.

Similar to phosphorus concentrations, variations in nitrogen availability from the mesophotic to the lower-rariphotic depths may also be a critical factor influencing the nitrogen metabolism of both demosponges and hexactinellids holobionts. Within the microbiomes of both classes, the AOA genus *Cenarchaeum* was specifically associated with the lower-rariphotic, suggesting a preference for habitats with elevated ammonium concentrations. This genus is represented by the species *Cenarchaeum symbiosum*, the first archaeal symbiont identified in sponges, originally discovered in the marine sponge *Dragmacidon mexicanum* (as *Axinella mexicana* in Preston et al. [99]). This widespread sponge symbiont is known for its role in ammonia detoxification through ammonia oxidation [27, 100, 101]. We propose that *Cenarchaeum* plays a crucial role in supporting lower-rariphotic sponge holobionts by facilitating ammonia detoxification, particularly under the challenging conditions of the oxygen minimum zone (OMZ), which occurs at similar depths (Fig. 6E).

Our metabolomics analysis revealed a diverse range of dipeptides, and amino sugar (e.g., rhodosamine) that varied in normalized concentrations across photic zones in both demosponges and hexactinellids. These compounds are critical components of dissolved organic nitrogen (DON) in coral- and algae-dominated reef ecosystems [102, 103]. Amino acid transporters have been identified in several bacterial metagenomes of sponge symbionts, enabling the uptake of a wide diversity of carbon and nitrogen sources potentially produced by the sponge host [16, 104–106]. Additionally, amino acids can be synthesized by the sponge host and subsequently metabolized by symbionts, as suggested by a transcriptomics analysis on *Xestospongia muta* [102]. Our multi-omics analysis highlights a co-occurrence of dipeptides and amino sugars together with several Chloroflexi and Acidobacteriota ASVs in demosponges. Notably, Chloroflexi (including the SAR202) are frequently implicated in the dissolved organic matter DOM cycling across shallow [107, 108], subtidal caves [109], mesophotic [34] and deep-sea ecosystems [110–112]. These co-occurrences suggest that these microbial groups may play a key role in the cycling of dipeptides and amino sugars, contributing to the DON pool within demosponges holobionts across all depth zones (Fig. 6F). Within the dipeptide family, higher concentrations were detected in lower-rariphotic demosponges and upper-rariphotic hexactinellids (Fig. 6F).

Further research is needed to explore how these dipeptide distribution patterns, both class- and zone-specific, may reflect distinct strategies for DON cycling in response to the seawater chemistry unique to each zone. For example, shotgun metagenomics and metatranscriptomics could be considered to better characterize the metabolic capabilities of sponge-associated prokaryotes. Additionally, a limit of this study might be linked to the preservation of labile metabolites (which might constitute an important diversity of the DOM pool) and DNA in ethanol, and the flash-freezing conservation method has to be considered. Such analyses performed across depth, but also space and time combined with a dedicated monitoring of the physico-chemical parameters, could clarify the specific effect of environmental factors. Additionally, the metabolic reliance of deep-sea sponge symbionts on nutrient exchange could also be studied through cultivation efforts, as observed with the spent metabolites from Ca. *Bathyarchaeia* enrichments facilitating the cultivation of previously unculturable bacteria from deep-ocean sediments [113].

Symbiotic strategies between rariphotic hexactinellid-holobionts and their associated fauna revealed by in-depth annotation of secondary metabolites

In addition to phospholipids and dipeptides, another major compound family identified in this study was dibrominated alkaloids, unexpectedly detected as biomarkers for hexactinellids. Typically, Demospongiae and their microbiome are well known for producing diverse halogenated compounds [114–119], but the biosynthesis of such compounds in Hexactinellida sponges has not been reported until now. Based on fragmentation pattern elucidation, this family of dibrominated alkaloids was identified as aphrocallistin and its derivatives. Aphrocallistin was initially isolated from extracts of the glass sponge *Aphrocallistes Beatrix* [72], but subsequent studies suggested it was produced by zoanthids colonizing the sponge specimens [120]. Our findings support this hypothesis, as aphrocallistin and its derivatives were detected in lower-rariphotic Hexactinellida species that were specifically colonized by zoanthids. These species were *V. liberatorii* and *C. pourtalesi*, and to a lesser extent *Hexactinella* sp. (Fig. 6G). These zoanthids were identified as *Vitrumanthus schrieri* across all three glass-sponge species. The identification aligns with previous findings of *V. schieri* associated with hexactinellids (*V. liberatorii* and *Cyrtaulon sigsbeei*) collected in Curaçao [33, 121]. Interestingly, Caribbean specimens of *Aphrocallistes beatrix* have also been reported in association with the zoanthid *Vitrumanthus vanderlandi* [121]. This suggests that the production of aphrocallistin may not be limited to a specific zoanthid species, but could be a characteristic of the genus *Vitrumanthus*. Recent studies highlight that the extensive diversity of deep-sea zoanthids living as epibionts of Hexactinellida sponges remains largely unexplored [121–123]. These zoanthid-hexactinellid associations are often considered a form of symbiosis [121], and we propose that the production of aphrocallistins by zoanthids may serve as a source of chemical defense for the sponge host. In contrast, demosponges are well-known for hosting diverse bacterial symbionts with halogenation and dehalogenation activities [124], differentiating their chemical defense strategies from those of hexactinellids. For example, Cyanobacteria and Chloroflexi symbionts are known to participate in the bromination of inactive alkaloid precursors produced by the sponge host, leading to unique biosynthetic pathways for chemical defenses at the holobiont level [114, 125]. However, in this study, the absence of Chloroflexi in Hexactinellida (and Cyanobacteria in the lower-rariphotic ones), which are instead dominated by Ammonia-oxidizing Archaea (AOA), suggests that such bromination pathways are likely absent in hexactinellid holobionts such as *C. pourtalesi*. As a result, the symbiotic association with zoanthids producing bioactive dibrominated alkaloids may serve as an alternate chemical defense strategy for the hexactinellid sponges in deeper ecosystems (Fig. 6G). In exchange, these heavily encrusting zoanthids [121] may benefit from the natural filter-feeding activity of the sponge to support their own nutrition. The functional role of the microbiome in *C. pourtalesi* and *V. liberatorii* both dominated by distinct *Cenarchaeum* symbionts remains to be fully explored. However, the production of aphrocallistin by zoanthids appears to be independent of the sponge's microbial community structure. For instance, *A. beatrix* was dominated by the AOA Candidatus *Nitrosoabyssus spongiisocia* and the gammaproteobacterial Candidatus *Zeuxoniibacter abyssi* [126], and yet still associated with these zoanthids.

In addition to aphrocallistins, the detection of xanthurenic acid (XA) provides another example of secondary metabolites involved in hexactinellid-fauna associations (Fig. 6H). Specifically, XA has been previously isolated from extracts of the Antarctica sea sponge *Isodictya erinaceae* and identified as an endogenous molt inhibitor in crustaceans, such as the amphipod *Pseudorchomene plebs* [127], as well as in various crab species [128–130]. Our results revealed higher concentrations of XA in *C. pourtalesi* samples. Notably, several specimens of this sponge species were found to harbor shrimp pairs within their internal cavities during subsampling. Based on morphological analysis, these shrimp were identified as *Eiconaxius caribbaeus* (Faxon, 1896 pers. observ. Charles Fransen). Adult shrimp of the genus *Eiconaxius* are known to exclusively inhabit the internal canals and

cavities of deep-sea hexactinellid sponges [131]. Therefore, it is plausible that these shrimps produce XA as an endogenous hormone to regulate their body size, enabling them to remain small enough to occupy the sponge's internal cavities, which are approximately 5 mm in diameter.

Results from our untargeted metabolomics approach highlight the importance of comprehensive annotation strategies when analyzing complex sponge holometabolomes, as well as those of other marine models [71, 81]. These efforts have revealed diverse symbiotic strategies uncovering potential interactions between sponge holobionts and their associated fauna. While the production of aphrocallistins by the zoanthids might indicate a novel defense strategy within sponges, the presence of xanthurenic acid could provide an ecological context associated with the growth limits of shrimps inhabiting sponge cavities. These findings exemplify the "nested ecosystems" concept, emphasizing the need to integrate multiple ecological scales to fully understand the intricate relationships within sponge-holobionts and their interactions with the broader environment [14]. By identifying a unique diversity of secondary metabolites within hexactinellid holobionts and their associated fauna, our study underscores the need for deeper exploration of chemical interactions within rariphotic assemblages. Such investigations pave the way for the discovery of new natural products, as demonstrated by the potential of aphrocallistin in cancer treatment research [72, 132]. Moreover, these findings highlight the critical importance of preserving these unique ecosystems, through dedicated conservation efforts [30].

Conclusions

Our study revealed distinct adaptive strategies of sponge holobionts across and below the mesophotic zone, driven by host-microbiome interactions, depth-related environmental factors, and the production of unique secondary metabolites.

Using a multi-omics approach, we identified significant differences in microbial community structure and holometabolome diversity between Demospongiae and Hexactinellida sponges, indicating limited functional redundancy between these classes. Consistent with findings in other benthic communities, our results also support a clear delineation between mesophotic and rariphotic zones for demosponges, reflecting distinct adaptive strategies at the holobiont level. Depth-specific patterns in microbial and chemical markers (such as membrane phospholipid adaptations and nitrogen metabolism processes) underscore the potential influence of environmental gradients (e.g., temperature, pressure, and nutrient availability) in shaping these holobionts. Furthermore, the detection of secondary metabolites such as aphrocallistin and xanthurenic acid, which are associated with symbiotic fauna, reveals novel ecological strategies in rariphotic hexactinellids. These findings highlight the intricate symbiotic relationships between sponge holobionts and their associated fauna, supporting the concept of sponge holobionts as integral components of a nested ecosystem.

Supplementary Information

The online version contains supplementary material available at https://doi.org/10.1186/s40168-025-02146-2.

Table S1. Summary of the sample list. The color corresponds to the color codes used for all figures. Table S2. Results of the two-way PERMANOVA tests conducted with the sponge class and the photic zone factors, for both metabarcoding and metabolomics datasets. Table S3. Results of the multivariate pairwise adonis test comparing five groups of sponge samples gathered according to their sponge class and photic zone, for both metabarcoding and metabolomics datasets. Table S4. Results of the nested PERMANOVA tests conducted with the "sponge genus" factor nested within each "sponge class" factor, for both metabarcoding and metabolomics datasets. Table S5. Summarized results of the significant multivariate pairwise adonis comparisons within sponge genus, for both metabarcoding and metabolomics datasets. Table S6. Summary of the differential analyses conducted on the metabarcoding (phylogenetical heat trees) and metabolomics (PLS-DA) datasets. Table S7. List of biomarker metabolites (VIP score > 2) annotated by LC-HRMS/MS and involved in the discriminations between the two sponge classes (Demospongiae vs Hexactinellida). Table S8. List of biomarker metabolites (VIP score > 3) annotated by LC-HRMS/MS and involved in the photic zone discriminations for the Demospongiae samples. Table S9. List of biomarker metabolites (VIP score > 3) annotation by LC-HRMS/MS and involved in the photic zone discriminations for the Hexactinellida samples. Figure S1. Workflow of the complementary approaches, combining 16S and 28S rRNA gene barcoding of sponges, 16S rRNA gene metabarcoding of the microbiome, UHPLC-MS metabolomics of holometabolome. Figure S2. Map of the sampling site. A. Location of Curaçao and bathymetry data. B. Detailed map of the study area. Figure S3. Pictures of collected sponge specimens. Figure S4. Pictures of the hexactinellid-associated fauna.Figure S5. α-diversity analysis of the sponge-associated prokaryotic communities and holometabolomes. Figure S6. Barplots of the prokaryotic community composition at the family level associated with the Demospongiae and Hexactinellida samples in their respective photic zones (mesophotic, upper rariphotic, and lower rariphotic). Figure S7. Barplots of the archaeal community composition at the genus level associated with the Demospongiae and Hexactinellida samples in their respective photic zones (mesophotic, upper rariphotic, and lower rariphotic). Figure S8. Phylogenetical heat tree representing the taxa significantly and differentially abundant between Demospongiae and Hexactinellida samples. Figure S9. Phylogenetical heat trees performed with Hexactinellida samples, and representing taxa significantly and differentially abundant between upper and lower rariphotic samples. Figure S10. PLS-DA plots of the holometabolomes conducted with the photic zone as a supervised factor, for both Demospongiae (A) and Hexactinellida (B) subseted datasets. Figure S11. FBMN analysis. Figure S12. Annotation of phospholipids identified within clusters A and D. Abbreviations: PC: phosphatidylcholine; PE: for phosphatidylethanolamine. Figure S13. Annotation of brominated compounds identified within clusters D and G. Figure S14. HRMS/MS data (A) and putative MS fragmentation (B) of VIP n°13 identified as aphrocallistin (Wright et al., 2009). Figure S15. Normalized concentrations of VIP n°13, 25, and 28, identified as aphrocallistin, an aphrocallistin derivative, and xanthurenic acid, respectively. Figure S16. HRMS/MS data and match with the GNPS Library Spectrum CCMSLIB of VIP n°27 identified as xanthurenic acid. Figure S17. Barplots of the archaeal community composition obtained with 6 of the Hexactinellida samples with (A) the 515F-Y-926R primers (Parada et al., 2016), and (B) archaeal-specific Uni519F-1000R primers (Ovreås et al., 1997; Kolganova et al., 2002).

Acknowledgements
A special thanks goes to Adriaan "Dutch" Schrier for giving us the opportunity to use the 'Curasub' submarine, and the submarine pilots Bruce Brandt, and Tico Christiaanse for making the expedition run smoothly. We also thank Jeroen van Kuijk, Alexander Swaen, Kristina Beemsterboer and Stijn Raemaekers who helped during the sampling at Curaçao. We are also grateful to Pierre-Etienne Choley for his help on the nanopore data processing, and Sam Afoullouss for the confirmation of aphrocallistin identification based on the MS/MS fragmentation. We also acknowledge Charles Fransen and Werner de Gier for the identification of the crustacean specimens.

Authors' contributions
BP and NdV designed the study. BP, NdV, and NW performed the fieldwork. AT and BP performed the lab work for the 16S metabarcoding. AT, BP, and NW performed the 28S barcoding of Demospongiae samples. NdV performed the lab work for the morphological identification of the Demospongiae samples. CD performed the 16S barcoding of the Hexactinellida samples. CD and NdV performed the morphological identification of the Hexactinellida samples. AT and OE performed the lab work for the metabolomics study. BP and AT analyzed the metabarcoding results. YHC and OE designed the metabolomics experiments. AT, OE, and BP processed the metabolomics raw data. BP analyzed and annotated the metabolomics results. BP performed the multi-omics data integration and analyzed the results. BP and NdV wrote the first draft of the manuscript. All co-authors read, contributed to the revision, and approved the submitted version.

Funding
This work was funded by the NWO-VIDI with project number 16.161.301.

Data availability
16S rRNA gene sequences for metabarcoding were deposited and are publicly available in the NCBI Sequences Read Archive (SRA) under the BioProject ID PRJNA1216067, accession number. MS data are available in the Mass Spectrometry Interactive Virtual Environment (MassIVE) repository MSV000096962. FBMN workflows can be accessed in GNPS with the following links: https://gnps.ucsd.edu/ProteoSAFe/status.jsp?task=b9d95e6d74bd4428abe42b5667028897. The R scripts used for all the 16S rRNA gene metabarcoding, metabolomics, and multi-omics analyses can be found at https://github.com/BenoitPAIX/Rariphotic_sponge_microbiomes. Sequences for sponge and associated fauna barcoding were deposited and are publicly available in GenBank under the accession numbers from PV072791 to PV072818, and PV104008 to PV104031, for 16S and 28S rRNA genes respectively.

Declarations

Ethics approval and consent to participate
Not applicable

Consent for publication
Not applicable.

Competing interests
The authors declare no competing interests.

Received: 16 February 2025 Accepted: 19 May 2025
Published online: 02 July 2025

References

1. de Goeij JM, van Oevelen D, Vermeij MJA, Osinga R, Middelburg JJ, de Goeij AFPM, et al. Surviving in a marine desert: the sponge loop retains resources within coral reefs. Science. 2013;342:108–10.
2. Pawlik JR, McMurray SE. The emerging ecological and biogeochemical importance of sponges on coral reefs. Ann Rev Mar Sci. 2020;12:315–37.
3. Goren L, Idan T, Shefer S, Ilan M. Sponge-associated polychaetes: not a random assemblage. Front Mar Sci. 2021;8. Available from: https://www.frontiersin.org/journals/marine-science/articles/10.3389/fmars.2021.695163/full. Cited 2025 Jan 20.
4. Ilan M, Loya Y, Kolbasov GA, Brickner I. Sponge-inhabiting barnacles on Red Sea coral reefs. Mar Biol. 1999;133:709–16.
5. Kandler NM, Wooster MK, Leray M, Knowlton N, de Voogd NJ, Paulay G, et al. Hyperdiverse macrofauna communities associated with a common sponge, Stylissa carteri, shift across ecological gradients in the Central Red Sea. Diversity. 2019;11:18.
6. Thomas T, Moitinho-Silva L, Lurgi M, Björk JR, Easson C, Astudillo-García C, et al. Diversity, structure and convergent evolution of the global sponge microbiome. Nat Commun. 2016;7:11870.
7. Webster NS, Thomas T. The sponge hologenome mBio. 2016;7:e00135-e116.
8. Rosenberg E, Zilber-Rosenberg I. The hologenome concept of evolution after 10 years. Microbiome. 2018;6:78.
9. Zilber-Rosenberg I, Rosenberg E. Role of microorganisms in the evolution of animals and plants: the hologenome theory of evolution. FEMS Microbiol Rev. 2008;32:723–35.
10. Zilber-Rosenberg I, Rosenberg E. Microbial-driven genetic variation in holobionts. FEMS Microbiology Reviews. 2021;45:fuab022.
11. Wilkinson CR, Fay P. Nitrogen fixation in coral reef sponges with symbiotic cyanobacteria. Nature. 1979;279:527–9.
12. Fan L, Reynolds D, Liu M, Stark M, Kjelleberg S, Webster NS, et al. Functional equivalence and evolutionary convergence in complex communities of microbial sponge symbionts. Proc Natl Acad Sci. 2012;109:E1878–87.
13. Hardoim CCP, Costa R. Temporal dynamics of prokaryotic communities in the marine sponge Sarcotragus spinosulus. Mol Ecol. 2014;23:3097–112.
14. Pita L, Rix L, Slaby BM, Franke A, Hentschel U. The sponge holobiont in a changing ocean: from microbes to ecosystems. Microbiome. 2018;6:46.
15. Bell JJ, Davy SK, Jones T, Taylor MW, Webster NS. Could some coral reefs become sponge reefs as our climate changes? Glob Change Biol. 2013;19:2613–24.
16. Botté ES, Nielsen S, Abdul Wahab MA, Webster J, Robbins S, Thomas T, et al. Changes in the metabolic potential of the sponge microbiome under ocean acidification. Nat Commun. 2019;10:4134.
17. Posadas N, Baquiran JIP, Nada MAL, Kelly M, Conaco C. Microbiome diversity and host immune functions influence survivorship of sponge holobionts under future ocean conditions. ISME J. 2022;16:58–67.
18. Rix L, de Goeij JM, van Oevelen D, Struck U, Al-Horani FA, Wild C, et al. Differential recycling of coral and algal dissolved organic matter via the sponge loop. Funct Ecol. 2017;31:778–89.
19. Bart MC, Hudspith M, Rapp HT, Verdonschot PFM, de Goeij JM. A Deep-sea sponge loop? Sponges transfer dissolved and particulate organic carbon and nitrogen to associated fauna. Front Mar Sci. 2021;8. Available from: https://www.frontiersin.org/journals/marine-science/articles/10.3389/fmars.2021.604879/full. Cited 2025 Jan 20.
20. Steinert G, Busch K, Bayer K, Kodami S, Arbizu PM, Kelly M, et al. Compositional and quantitative insights into bacterial and archaeal communities of South Pacific deep-sea sponges (Demospongiae and Hexactinellida). Front Microbiol. 2020;11. Available from: https://www.frontiersin.org/journals/microbiology/articles/10.3389/fmicb.2020.00716/full. Cited 2025 Jan 20.
21. Garritano AN, Majzoub ME, Ribeiro B, Damasceno T, Modolon F, Messias C, et al. Species-specific relationships between deep sea sponges and their symbiotic Nitrosopumilaceae. ISME J. 2023;1–3.
22. Díez-Vives C, Riesgo A. High compositional and functional similarity in the microbiome of deep-sea sponges. The ISME Journal. 2024;18:wrad030.
23. Moitinho-Silva L, Steinert G, Nielsen S, Hardoim CCP, Wu Y-C, McCormack GP, et al. Predicting the HMA-LMA status in marine sponges by machine learning. Front Microbiol. 2017;8:752.
24. Cleary DFR, de Voogd NJ, Stuij TM, Swierts T, Oliveira V, Polónia ARM, et al. A Study of Sponge Symbionts from Different Light Habitats. Microb Ecol. 2023;86:2819–37.
25. Tian R, Sun J, Cai L, Zhang W, Zhou G, Qiu J, et al. The deep-sea glass sponge *Lophophysema eversa* harbours potential symbionts responsible for the nutrient conversions of carbon, nitrogen and sulfur. Environ Microbiol. 2016;18:2481–94.
26. Busch K, Slaby BM, Bach W, Boetius A, Clefsen I, Colaço A, et al. Biodiversity, environmental drivers, and sustainability of the global deep-sea sponge microbiome. Nat Commun. 2022;13:5160.

27. Bayer K, Busch K, Kenchington E, Beazley L, Franzenburg S, Michels J, et al. Microbial strategies for survival in the glass sponge Vazella pourtalesii. mSystems. 2020;5. https://doi.org/10.1128/msystems.00473-20.
28. Baldwin CC, Tornabene L, Robertson DR. Below the mesophotic Sci Rep. 2018;8:4920.
29. Semmler RF, Hoot WC, Reaka ML. Are mesophotic coral ecosystems distinct communities and can they serve as refugia for shallow reefs? Coral Reefs. 2017;36:433–44.
30. Stefanoudis PV, Rivers M, Smith SR, Schneider CW, Wagner D, Ford H, et al. Low connectivity between shallow, mesophotic and rariphotic zone benthos. Royal Society Open Science. 2019;6: 190958.
31. van Soest R. A Checklist of the Curaçao Sponges (Porifera Demospongiae) including a pictorial key to the more common reef-forms. Verslagen en Technische Gegevens. 1981;31:1–39.
32. van Soest RWM, Meesters EHWG, Becking LE. Deep-water sponges (Porifera) from Bonaire and Klein Curaçao. Southern Caribbean Zootaxa. 2014;3878:401–43.
33. Reiswig HM, Dohrmann M. Three new species of glass sponges (Porifera: Hexactinellida) from the West Indies, and molecular phylogenetics of Euretidae and Auloplacidae (Sceptrulophora). Zool J Linn Soc. 2014;171:233–53.
34. Cleary DFR, van Bendegom DJ, Gomes NCM, de Voogd NJ. Sponge-associated microbes in the twilight zone of Curaçao. Symbiosis. 2024;93:81–97.
35. Robertson DR, Tornabene L, Lardizabal CC, Baldwin CC. Submersibles greatly enhance research on the diversity of deep-reef fishes in the Greater Caribbean. Front Mar Sci. 2022;8. Available from: https://www.frontiersin.org/journals/marine-science/articles/10.3389/fmars.2021.800250/full. Cited 2024 Jul 25.
36. Reiswig HM, Stone RP. New glass sponges (Porifera: Hexactinellida) from deep waters of the central Aleutian Islands, Alaska. Zootaxa. 2013;3628. Available from: https://mapress.com/zt/article/view/zootaxa.3628.1.1. Cited 2025 Jan 31.
37. Reiswig HM. Class Hexactinellida Schmidt, 1870. pp 1201–1210. In: Hooper, J.N.A. & van Soest, R.W.M. (2002 [2004]). Systema Porifera. A guide to the classification of sponges (2 volumes). Kluwer Academic/Plenum, NY. 1708 + XLVIII. ISBN 978–1–4615–0747–5 (eBook electronic version). 2002. Available from: https://www.marinespecies.org/porifera/porifera.php?p=sourcedetails&id=404600. Cited 2025 Jan 31.
38. de Voogd N, Alvarez B, Boury-Esnault N, Cárdenas P, Díaz M-C, Dohrmann M, et al. World Porifera Database. Accessed at https://www.marinespecies.org/porifera on yyyy-mm-dd. VLIZ; 2025. Available from: https://www.marinespecies.org/imis.php?dasid=546&id=359. Cited 2025 Jan 21.
39. Chombard C, Boury-Esnault N, Tillier S. Reassessment of homology of morphological characters in tetractinellid sponges based on molecular data. Syst Biol. 1998;47:351–66.
40. Maslin M, Paix B, van der Windt N, Ambo-Rappe R, Debitus C, Gaertner-Mazouni N, et al. Prokaryotic communities of the French Polynesian sponge *Dactylospongia metachromia* display a site-specific and stable diversity during an aquaculture trial. Antonie Van Leeuwenhoek. 2024;117:65.
41. Dohrmann M, Voigt O, Erpenbeck D, Wörheide G. Non-monophyly of most supraspecific taxa of calcareous sponges (Porifera, Calcarea) revealed by increased taxon sampling and partitioned Bayesian analysis of ribosomal DNA. Mol Phylogenet Evol. 2006;40:830–43.
42. Bridge D, Cunningham CW, Schierwater B, DeSalle R, Buss LW. Class-level relationships in the phylum Cnidaria: evidence from mitochondrial genome structure. Proc Natl Acad Sci USA. 1992;89:8750–3.
43. Dohrmann M, Janussen D, Reitner J, Collins AG, Wörheide G. Phylogeny and Evolution of Glass Sponges (Porifera, Hexactinellida). Syst Biol. 2008;57:388–405.
44. Parada AE, Needham DM, Fuhrman JA. Every base matters: assessing small subunit rRNA primers for marine microbiomes with mock communities, time series and global field samples. Environ Microbiol. 2016;18:1403–14.
45. Ovreås L, Forney L, Daae FL, Torsvik V. Distribution of bacterioplankton in meromictic Lake Saelenvannet, as determined by denaturing gradient gel electrophoresis of PCR-amplified gene fragments coding for 16S rRNA. Appl Environ Microbiol. 1997;63:3367–73.
46. Takahashi S, Tomita J, Nishioka K, Hisada T, Nishijima M. Development of a prokaryotic universal primer for simultaneous analysis of bacteria and archaea using next-generation sequencing. PLoS ONE. 2014;9: e105592.
47. Callahan BJ, McMurdie PJ, Rosen MJ, Han AW, Johnson AJA, Holmes SP. DADA2: High-resolution sample inference from Illumina amplicon data. Nat Methods. 2016;13:581–3.
48. Callahan BJ, McMurdie PJ, Holmes SP. Exact sequence variants should replace operational taxonomic units in marker-gene data analysis. ISME J. 2017;11:2639–43.
49. Callahan BJ, Sankaran K, Fukuyama JA, McMurdie PJ, Holmes SP. Bioconductor workflow for microbiome data analysis: from raw reads to community analyses [Internet]. F1000Research; 2016 [cited 2022 Feb 23]. Available from: https://f1000research.com/articles/5-1492
50. Quast C, Pruesse E, Yilmaz P, Gerken J, Schweer T, Yarza P, et al. The SILVA ribosomal RNA gene database project: improved data processing and web-based tools. Nucleic Acids Res. 2013;41:D590–6.
51. Parks DH, Chuvochina M, Waite DW, Rinke C, Skarshewski A, Chaumeil P-A, et al. A standardized bacterial taxonomy based on genome phylogeny substantially revises the tree of life. Nat Biotechnol. 2018;36:996–1004.
52. McMurdie PJ, Holmes S. phyloseq: an R package for reproducible interactive analysis and graphics of microbiome census data. PLoS ONE. 2013;8: e61217.
53. Davis NM, Proctor DM, Holmes SP, Relman DA, Callahan BJ. Simple statistical identification and removal of contaminant sequences in marker-gene and metagenomics data. Microbiome. 2018;6:226.
54. Oksanen J, Blanchet FG, Friendly M, Kindt R, Legendre P, McGlinn D, et al. vegan: Community ecology package. 2019. Available from: https://CRAN.R-project.org/package=vegan. Cited 2020 Jan 15.
55. Mendiburu F de. Agricolae: Statistical procedures for agricultural research. 2019. Available from: https://CRAN.R-project.org/package=agricolae. Cited 2019 Jul 9.
56. McMurdie PJ, Holmes S. Waste not, want not: why rarefying microbiome data is inadmissible. PLoS Comput Biol. 2014;10: e1003531.
57. Gloor GB, Macklaim JM, Pawlowsky-Glahn V, Egozcue JJ. Microbiome datasets are compositional: and this is not optional. Front Microbiol. 2017;8:2224.
58. Foster ZSL, Sharpton TJ, Grünwald NJ. Metacoder: An R package for visualization and manipulation of community taxonomic diversity data. PLoS Comput Biol. 2017;13: e1005404.
59. Paix B, Layglon N, Poupon CL, D'Onofrio S, Misson B, Garnier C, et al. Integration of spatio-temporal variations of surface metabolomes and epibacterial communities highlights the importance of copper stress as a major factor shaping host-microbiota interactions within a Mediterranean seaweed holobiont. Microbiome. 2021;9. Available from: https://doi.org/10.1186/s40168-021-01124-8. Cited 2021 Oct 19.
60. Pang Z, Lu Y, Zhou G, Hui F, Xu L, Viau C, et al. MetaboAnalyst 6.0: towards a unified platform for metabolomics data processing, analysis and interpretation. Nucleic Acids Research. 2024;52:W398–406.
61. Wang M, Carver JJ, Phelan VV, Sanchez LM, Garg N, Peng Y, et al. Sharing and community curation of mass spectrometry data with Global Natural Products Social Molecular Networking. Nat Biotechnol. 2016;34:828–37.
62. Schymanski EL, Jeon J, Gulde R, Fenner K, Ruff M, Singer HP, et al. Identifying small molecules via high resolution mass spectrometry: communicating confidence. Environ Sci Technol. 2014;48:2097–8.
63. Kassambara A. ggpubr:'ggplot2'based publication ready plots. R package version. 2018;2.
64. Lê Cao K-A, González I, Déjean S. integrOmics: an R package to unravel relationships between two omics datasets. Bioinformatics. 2009;25:2855–6.
65. Rohart F, Gautier B, Singh A, Cao K-AL. mixOmics: an R package for 'omics feature selection and multiple data integration. PLOS Computational Biology. 2017;13:e1005752.
66. Schmidt O. Die Spongien des Meerbusen von Mexico (Und des caraibischen Meeres). Heft II. Abtheilung II. Hexactinelliden. Abtheilung III. Tetractinelliden. Monactinelliden und Anhang. Nachträge zu Abtheilung I (Lithistiden). Pp. 33–90, pls V-X. In: Reports on the dredging under the supervision of Alexander Agassiz, in the Gulf of Mexico, by the USCSS 'Blake'. (Gustav Fischer:Jena). 1880. Available from: https://www.marinespecies.org/porifera/porifera.php?p=sourcedetails&id=8186. Cited 2025 Jan 27.

67. Uliczka E. Die tetraxonen Schwämme Westindiens (auf Grund der Ergebnisse der Reise Kükenthal-Hartmeyer). Pp. 35–62. In: Kükenthal, W. & Hartmeyer, R. (Eds), Ergebnisse einer zoologischen Forschungsreise nach Westindien. Zoologische Jahrbücher. Abteilung für Systematik, Geographie und Biologie der Thiere, Supplement 16. 1929. Available from: https://www.marinespecies.org/aphia.php?p=sourcedetails&id=8421. Cited 2025 Jan 27.
68. Alvarez B, van Soest RWM, Rützler K. A Revision of Axinellidae (Porifera: Demospongiae) in the Central West Atlantic Region. Smithsonian Contribution to Zoology. 1998;598:1–47.
69. de Laubenfels MW. New sponges from the Puerto Rican deep. Smithsonian Miscellaneous Collections. 1934;91:1–28.
70. Faxon W. Reports on the results of dredging, under the supervision of Alexander Agassiz, in the Gulf of Mexico and the Caribbean Sea, and on the East Coast of the United States, 1877 to 1880, by the U.S. Coast Survey Steamer "Blake", Lieut.-Commander C.D. Sigsbee, U.S.N., and Commander J.R.Bartlett, U.S.N., commanding. XXXVII. Supplementary notes on the Crustacea. Bulletin of the Museum of comparative Zoology at Harvard College. 1896; Available from: https://marinespecies.org/aphia.php?p=sourcedetails&id=144448. Cited 2025 Jan 27.
71. Carriot N, Paix B, Greff S, Viguier B, Briand J-F, Culioli G. Integration of LC/MS-based molecular networking and classical phytochemical approach allows in-depth annotation of the metabolome of non-model organisms - The case study of the brown seaweed *Taonia atomaria*. Talanta. 2021;225: 121925.
72. Wright AE, Roth GP, Hoffman JK, Divlianska DB, Pechter D, Sennett SH, et al. Isolation, synthesis, and biological activity of Aphrocallistin, an adenine-substituted bromotyramine metabolite from the Hexactinellida sponge Aphrocallistes beatrix. J Nat Prod. 2009;72:1178–83.
73. Godzien J, Ciborowski M, Martínez-Alcázar MP, Samczuk P, Kretowski A, Barbas C. Rapid and reliable identification of phospholipids for untargeted metabolomics with LC–ESI–QTOF–MS/MS. J Proteome Res. 2015;14:3204–16.
74. Mazzella V, Dell'Anno A, Etxebarría N, González-Gaya B, Nuzzo G, Fontana A, et al. High microbiome and metabolome diversification in coexisting sponges with different bio-ecological traits. Commun Biol. 2024;7:1–18.
75. Lesser MP, Sabrina Pankey M, Slattery M, Macartney KJ, Gochfeld DJ. Microbiome diversity and metabolic capacity determines the trophic ecology of the holobiont in Caribbean sponges. ISME COMMUN. 2022;2:1–12.
76. Galand PE, Pereira O, Hochart C, Auguet JC, Debroas D. A strong link between marine microbial community composition and function challenges the idea of functional redundancy. ISME J. 2018;12:2470–8.
77. Dohrmann M, Reiswig HM, Kelly M, Mills S, Schätzle S, Reverter M, et al. Expanded sampling of New Zealand glass sponges (Porifera: Hexactinellida) provides new insights into biodiversity, chemodiversity, and phylogeny of the class. PeerJ. 2023;11: e15017.
78. Genin E, Wielgosz-Collin G, Njinkoué J-M, Velosaotsy NE, Kornprobst J-M, Gouygou J-P, et al. New trends in phospholipid class composition of marine sponges. Comp Biochem Physiol B: Biochem Mol Biol. 2008;150:427–31.
79. Torkhovskaya TI, Ipatova OM, Zakharova TS, Kochetova MM, Khalilov EM. Lysophospholipid receptors in cell signaling. Biochemistry Moscow. 2007;72:125–31.
80. Ivanisevic J, Pérez T, Ereskovsky AV, Barnathan G, Thomas OP. Lysophospholipids in the Mediterranean sponge Oscarella tuberculata: seasonal variability and putative biological role. J Chem Ecol. 2011;37:537–45.
81. Reverter M, Tribalat M-A, Pérez T, Thomas OP. Metabolome variability for two Mediterranean sponge species of the genus Haliclona: specificity, time, and space. Metabolomics. 2018;14:114.
82. Zhang S, Song W, Nothias L-F, Couvillion SP, Webster N, Thomas T. Comparative metabolomic analysis reveals shared and unique chemical interactions in sponge holobionts. Microbiome. 2022;10:22.
83. Sugiura T, Fukuda T, Miyamoto T, Waku K. Distribution of alkyl and alkenyl ether-linked phospholipids and platelet-activating factor-like lipid in various species of invertebrates. Biochimica et Biophysica Acta (BBA) - Lipids and Lipid Metabolism. 1992;1126:298–308.
84. Mannochio-Russo H, Swift SOI, Nakayama KK, Wall CB, Gentry EC, Panitchpakdi M, et al. Microbiomes and metabolomes of dominant coral reef primary producers illustrate a potential role for immunolipids in marine symbioses. Commun Biol. 2023;6:1–19.
85. Müller WEG, Klemt M, Thakur NL, Schröder HC, Aiello A, D'Esposito M, et al. Molecular/chemical ecology in sponges: evidence for an adaptive antibacterial response in Suberites domuncula. Mar Biol. 2004;144:19–29.
86. Butler AJ, van Altena IA, Dunne SJ. Antifouling activity oflyso-platelet-activating factor extracted from australian spongeCrella incrustans. J Chem Ecol. 1996;22:2041–61.
87. Cossins AR, Macdonald AG. The adaptation of biological membranes to temperature and pressure: fish from the deep and cold. J Bioenerg Biomembr. 1989;21:115–35.
88. Parzanini C, Parrish CC, Hamel J-F, Mercier A. Functional diversity and nutritional content in a deep-sea faunal assemblage through total lipid, lipid class, and fatty acid analyses. Loor JJ, editor. PLoS ONE. 2018;13:e0207395.
89. Winnikoff JR, Milshteyn D, Vargas-Urbano SJ, Pedraza-Joya MA, Armando AM, Quehenberger O, et al. Homeocurvature adaptation of phospholipids to pressure in deep-sea invertebrates. Science. 2024;384:1482–8.
90. Bennett H, Bell JJ, Davy SK, Webster NS, Francis DS. Elucidating the sponge stress response; lipids and fatty acids can facilitate survival under future climate scenarios. Glob Change Biol. 2018;24:3130–44.
91. Paytan A, McLaughlin K. The oceanic phosphorus cycle. Chem Rev. 2007;107:563–76.
92. Popendorf KJ, Tanaka T, Pujo-Pay M, Lagaria A, Courties C, Conan P, et al. Gradients in intact polar diacylglycerolipids across the Mediterranean Sea are related to phosphate availability. Biogeosciences. 2011;8:3733–45.
93. Zhang S, Song W, Wemheuer B, Reveillaud J, Webster N, Thomas T. Comparative genomics reveals ecological and evolutionary insights into sponge-associated thaumarchaeota. mSystems. 2019;4:e00288–19.
94. Wang P, Li M, Dong L, Zhang C, Xie W. Comparative genomics of thaumarchaeota from deep-sea sponges reveal their niche adaptation. Front Microbiol. 2022;13. Available from: https://www.frontiersin.org/journals/microbiology/articles/10.3389/fmicb.2022.869834/full. Cited 2025 Jan 27.
95. Glasl B, Luter HM, Damjanovic K, Kitzinger K, Mueller AJ, Mahler L, et al. Co-occurring nitrifying symbiont lineages are vertically inherited and widespread in marine sponges. The ISME Journal. 2024;wrae069.
96. Steger D, Ettinger-Epstein P, Whalan S, Hentschel U, De Nys R, Wagner M, et al. Diversity and mode of transmission of ammonia-oxidizing archaea in marine sponges. Environ Microbiol. 2008;10:1087–94.
97. Polónia ARM, Cleary DFR, Freitas R, de Voogd NJ, Gomes NCM. The putative functional ecology and distribution of archaeal communities in sponges, sediment and seawater in a coral reef environment. Mol Ecol. 2015;24:409–23.
98. Polónia ARM, Cleary DFR, Gauvin-Bialecki A, de Voogd NJ. Archaeal communities of low and high microbial abundance sponges inhabiting the remote western Indian Ocean island of Mayotte. Antonie Van Leeuwenhoek. 2021;114:95–112.
99. Preston CM, Wu KY, Molinski TF, DeLong EF. A psychrophilic crenarchaeon inhabits a marine sponge: Cenarchaeum symbiosum gen. nov., sp. nov. Proc Natl Acad Sci USA. 1996;93:6241–6.
100. Turque AS, Batista D, Silveira CB, Cardoso AM, Vieira RP, Moraes FC, et al. Environmental shaping of sponge associated archaeal communities. Steinke D, editor. PLoS ONE. 2010;5:e15774.
101. Hallam SJ, Konstantinidis KT, Putnam N, Schleper C, Watanabe Y, Sugahara J, et al. Genomic analysis of the uncultivated marine crenarchaeote *Cenarchaeum symbiosum*. Proc Natl Acad Sci USA. 2006;103:18296–301.
102. Fiore CL, Labrie M, Jarett JK, Lesser MP. Transcriptional activity of the giant barrel sponge, Xestospongia muta Holobiont: molecular evidence for metabolic interchange. Front Microbiol. 2015;6. Available from: https://www.frontiersin.org/articles/10.3389/fmicb.2015.00364/full#h3. Cited 2021 Jun 25.
103. Thobor BM, Haas AF, Wild C, Nelson CE, Wegley Kelly L, Hehemann J-H, et al. Coral high molecular weight carbohydrates support opportunistic microbes in bacterioplankton from an algae-dominated reef. mSystems. 2024;9:e00832–24.
104. Moitinho-Silva L, Díez-Vives C, Batani G, Esteves AI, Jahn MT, Thomas T. Integrated metabolism in sponge–microbe symbiosis revealed by genome-centered metatranscriptomics. ISME J. 2017;11:1651–66.

105. Podell S, Blanton JM, Oliver A, Schorn MA, Agarwal V, Biggs JS, et al. A genomic view of trophic and metabolic diversity in clade-specific Lamellodysidea sponge microbiomes. Microbiome. 2020;8:97.
106. Taylor JA, Palladino G, Wemheuer B, Steinert G, Sipkema D, Williams TJ, et al. Phylogeny resolved, metabolism revealed: functional radiation within a widespread and divergent clade of sponge symbionts. ISME J. 2021;15:503–19.
107. Bayer K, Jahn MT, Slaby BM, Moitinho-Silva L, Hentschel U. Marine sponges as Chloroflexi hot spots: genomic insights and high-resolution visualization of an abundant and diverse symbiotic clade. mSystems. 2018;3:e00150–18.
108. Maggioni F, Stenger P-L, Jourand P, Majorel C. The phylum Chloroflexi and their SAR202 clade dominate the microbiome of two marine sponges living in extreme environmental conditions. Mar Ecol. 2023;44: e12757.
109. Cleary DFR, Huang YM, Polónia ARM, van der Plas M, Gomes NCM, de Voogd NJ. Sponges and their prokaryotic communities sampled from a remote karst ecosystem. Mar Biodivers. 2024;54:8.
110. Busch K, Wurz E, Rapp HT, Bayer K, Franke A, Hentschel U. Chloroflexi dominate the deep-sea golf ball sponges *Craniella zetlandica* and *Craniella infrequens* throughout different life stages. Frontiers in Marine Science. 2020;7. Available from: https://www.frontiersin.org/articles/10.3389/fmars.2020.00674. Cited 2023 Dec 18.
111. Landry Z, Swan BK, Herndl GJ, Stepanauskas R, Giovannoni SJ. SAR202 genomes from the dark ocean predict pathways for the oxidation of recalcitrant dissolved organic matter. mBio. 2017;8:https://doi.org/10.1128/mbio.00413-17.
112. Campana S, Busch K, Hentschel U, Muyzer G, de Goeij JM. DNA-stable isotope probing (DNA-SIP) identifies marine sponge-associated bacteria actively utilizing dissolved organic matter (DOM). Environ Microbiol. 2021;23:4489–504.
113. Ishaq SE, Ahmad T, Liang L, Xie R, Yu T, Wang Y, et al. Cultivation of diverse novel marine bacteria from deep ocean sediment using spent culture supernatant of Ca. Bathyarchaeia enrichment J Microbiol. 2024;62:611–25.
114. Turon X, Becerro MA, Uriz MJ. Distribution of brominated compounds within the sponge Aplysina aerophoba : coupling of X-ray microanalysis with cryofixation techniques. Cell Tissue Res. 2000;301:311–22.
115. Kunze K, Niemann H, Ueberlein S, Schulze R, Ehrlich H, Brunner E, et al. Brominated skeletal components of the marine demosponges, Aplysina cavernicola and Ianthella basta: analytical and biochemical investigations. Mar Drugs. 2013;11:1271–87.
116. Lira NS, Montes RC, Tavares JF, da Silva MS, da Cunha EVL, de Athayde-Filho PF, et al. Brominated compounds from marine sponges of the genus Aplysina and a compilation of their 13C NMR spectral data. Mar Drugs. 2011;9:2316–68.
117. Ueberlein S, Machill S, Schupp PJ, Brunner E. Determination of the halogenated skeleton constituents of the marine demosponge Ianthella basta. Mar Drugs. 2017;15:34.
118. Agarwal V, Blanton JM, Podell S, Taton A, Schorn MA, Busch J, et al. Metagenomic discovery of polybrominated diphenyl ether biosynthesis by marine sponges. Nat Chem Biol. 2017;13:537–43.
119. Bayona LM, Kim M-S, Swierts T, Hwang G-S, de Voogd NJ, Choi YH. Metabolic variation in Caribbean giant barrel sponges: influence of age and sea-depth. Mar Environ Res. 2021;172: 105503.
120. Young RM. New apoptosome inhibitors from Irish deep-sea zoanthid. Poster in European Conference on Marine Natural Products 2021 (Galway). ECMNP; 2021. Available from: https://www.universityofgalway.ie/media/collegeofscience/schools/schoolofnaturalsciences/zoology/docs/ZoanthidPoster.pdf
121. Kise H, Montenegro J, Santos MEA, Hoeksema BW, Ekins M, Ise Y, et al. Evolution and phylogeny of glass-sponge-associated zoantharians, with a description of two new genera and three new species. Zool J Linn Soc. 2022;194:323–47.
122. Hajdu E, Castello-Branco C, Lopes DA, Sumida PYG, Perez JAA. Deep-sea dives reveal an unexpected hexactinellid sponge garden on the Rio Grande Rise (SW Atlantic). A mimicking habitat? Deep Sea Research Part II: Topical Studies in Oceanography. 2017;146:93–100.
123. Kahn AS, Pennelly CW, McGill PR, Leys SP. Behaviors of sessile benthic animals in the abyssal northeast Pacific Ocean. Deep Sea Res Part II. 2020;173: 104729.
124. Olinger LK, Strangman WK, McMurray SE, Pawlik JR. Sponges with microbial symbionts transform dissolved organic matter and take up organohalides. Front Mar Sci. 2021;8:548.
125. Sacristán-Soriano O, Banaigs B, Casamayor EO, Becerro MA. Exploring the links between natural products and bacterial assemblages in the sponge Aplysina aerophoba. Appl Environ Microbiol. 2011;77:862–70.
126. Garritano AN, Zhang Z, Jia Y, Allen MA, Hill LJ, Kuzhiumparambil U, et al. Simple Porifera holobiont reveals complex interactions between the host, an archaeon, a bacterium, and a phage. The ISME Journal. 2024;18:wrae197.
127. Vankayala SL, Kearns FL, Baker BJ, Larkin JD, Lee WH. Elucidating a chemical defense mechanism of Antarctic sponges: a computational study. J Mol Graph Model. 2017;71:104–15.
128. Ohnishi M, Naya Y. Effect of xanthurenic acid on P-450-dependent biotransformation by molting glands in vitro. Experientia. 1994;50:654–7.
129. Naya Y, Miki W, Ohnishi M, Ikeda M, Nakanishi K. Endogenous xanthurenic acid as a regulator of the crustacean molt cycle. Pure Appl Chem. 1989;61:465–8.
130. Naya Y, Ohnishi M, Ikeda M, Miki W, Nakanishi K. What is molt-inhibiting hormone? The role of an ecdysteroidogenesis inhibitor in the crustacean molting cycle. Proc Natl Acad Sci U S A. 1989;86:6826–9.
131. Kou Q, Xu P, Poore GCB, Li X, Wang C. A New Species of the Deep-Sea Sponge-Associated Genus Eiconaxius (Crustacea: Decapoda: Axiidae), With New Insights Into the Distribution, Speciation, and Mitogenomic Phylogeny of Axiidean Shrimps. Front Mar Sci. 2020;7. Available from: https://www.frontiersin.org/journals/marine-science/articles/10.3389/fmars.2020.00469/full. Cited 2025 Jan 28.
132. Wright AE, Sennett SH, Pomponi SA, McCarthy PJ, Guzman EA. Biologically active aphrocallistin compounds. 2011 . Available from: https://patents.google.com/patent/US8058430B2/en. Cited 2024 Nov 19.

Publisher's Note